Master Thesis

CFD Flow Field Study of a Hydrocyclone Operating under Non-Optimal Conditions

by Frank Bjerre Sørensen

Abstract

This master thesis is a study of the flow field inside a custom-made hydrocyclone using Computational Fluid Dynamics (CFD) while operating with different flow rates leading to non-optimal conditions. The RNG k-ε model is used to model the turbulence and the mixture model is used to model the multiphase and an experiment was carried out to validate the CFD model. The flow field study is carried out with a set Pressure Drop Ratio of 1.37, a fixed droplet size of 400μm, and flow rates from 0.4 to 0.8 L/s and the increasing flow rate showed an increase in separation efficiency. The flow field inside the hydrocyclone turned out to be unlike that of basic hydrocyclone theory; the overflow vortex was shown to origin relatively close to the hydrocyclone inlet and it was traveling along the hydrocyclone wall instead of the center. Increasing the flow rate will develop a longer overflow vortex and will therefore collect more oil from the oil core of the hydrocyclone, which is why the efficiency increases with the flow rate.

Frank Bjerre Sørensen

Project period: February 2^{nd} - June 9^{th} 2015
Supervisor: Matthias Mandø
MSc in Process Engineering and Combustion Technology, 10^{th} semester

Aalborg Universitet Esbjerg
Niels Bohrs Vej 8
6700 Esbjerg

Preface

This master thesis is made by Frank Bjerre Sørensen from Aalborg University in Esbjerg. It concludes the student's 10^{th} semester and education in the study of Process Engineering and Combustion Technology at Aalborg University, Esbjerg.

I would like to thank Petar Løhndorf for his support and for making this project possible by using the hydrocyclone he designed for his Ph.d. thesis. I would also like to thank Christian Mai and Simon Pedersen for their support and assistance provided to make the hydrocyclone setup suitable for my project. Finally I would like to thank my supervisor Matthias Mandø for his guidance and patience since day one in writing this thesis.

Contents

1 Project introduction

Hydrocyclones play an important role in many industries and can be used for numerous applications where separation is desired. Generally there are two types of hydrocyclones: liquid-liquid and liquid-solid hydrocyclones. The liquid-solid is probably the most used type, as many more applications apply to this. Examples of liquid-solid hydrocyclone applications include mineral processing and the separation of metal particles from cooling liquid in metal working. The liquid-liquid hydrocyclones are used in the oil industry for separating oil from water.

This project only considers the liquid-liquid hydrocyclone which operates with a mixture of water and oil. The importance of separation of these two phases comes from the official regulations which has set a maximum to the amount of parts per million (PPM) that can be in water that is to be flushed back into the sea or used for drilling purposes.

The subject in focus in this master thesis is the flow field inside a hydrocyclone using different inlet flow rates to see if any specific flow field changes occur when running the hydrocyclone at non-optimal conditions. This is not a subject that has previously been studied using Computational Fluid Dynamics, CFD. The intention is to simulate the flow using the same Pressure Drop Ratio, PDR, which is required to be controlled to keep a good separation through the hydrocyclone. By keeping a similar PDR for each flow rate, the flow field inside the hydrocyclone can be compared in a proper manner.

Aalborg University has a hydrocyclone setup in the laboratory in Esbjerg which is used to validate the CFD model. The setup consists of a custom made transparent plexiglass hydrocyclone block where the flow can be controlled using a centrifugal pump and the oil enters the system by a mixing valve. This setup is a part of a major setup which allows for a range of experiments and is mainly used by Petar Durdevic Løhndorf and Simon Pedersen to conduct their research project PDPWAC. The setup is not initially setup for thorough hydrocyclone testing with both water and oil, which is essential for this project and must be sorted out. To validate the model, an outlet mixture density and hydrocyclone inlet velocity will be compared to the experiment and the flows will be recorded using a camera and compared with the model.

Once the CFD model has been validated, it will be used to run simulations of several flow rates from 0.4 L/s to 0.8 L/s while keeping a PDR at 1.37. The tool used for the CFD simulation is ANSYS Fluent. This software is accepted as a solid CFD code which can solve most problem types and the possibilities for graphical illustrations of the results are perfect for this matter.

1.1 Limitations

This project is made with a set of limitations in order to keep the project within a reasonable size while still going through the necessary subjects to shed light on the problem.

- An optimal PDR is not known for this hydrocyclone as it is custom made and is still to be tested. This test is not performed for this project as the optimal hydrocyclone setup is not the scope of this project.
- A turbulence model study is not conducted as it is very time consuming. Data and results from other authors regarding this problem are used as references for this purpose.
- The cut size[1] of the hydrocyclone is not being determined in this project.

[1]The cut size of a hydrocyclone is defined as the size of the particle or droplets which is removed at 50% efficiency.

2 Introduction to Hydrocyclones

This chapter describes the operating principle and flow characteristics of hydrocyclones.

2.1 Background and operation principle

Hydrocyclones have been used for separation in the industry since the 1940's in many different applications ranging from pharmaceuticals to mineral processing and separation of oil and gas. The first patent on the hydrocyclone can be traced back to the nineteenth century[1]. This separation method is of a simple design and because there are no moving parts, operation is easy and the need for maintenance is low, which results in low cost.

The operational principle of hydrocyclones is fairly simple. Consider figure 2.1:

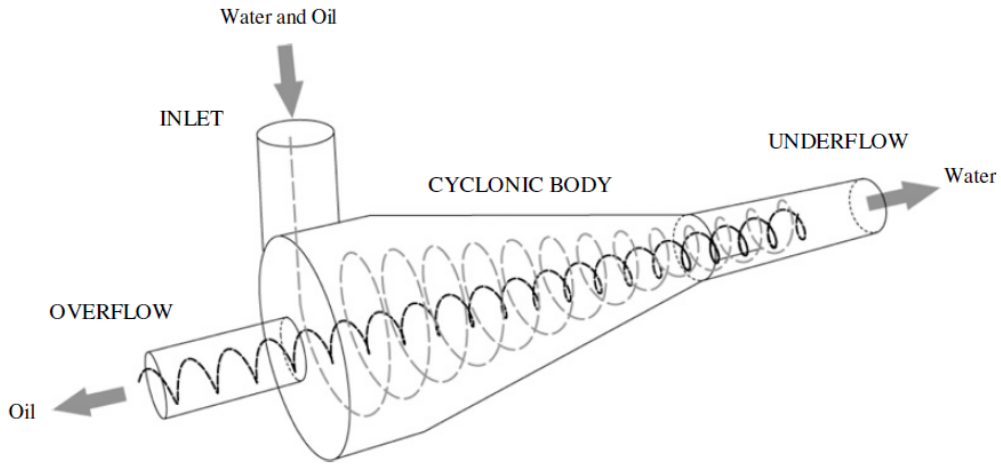

Figure 2.1: Hydrocyclone operating principle[2].

In a de-oiling hydrocyclone, a mixture of water and oil enters through the tangential inlet, which gives rise to a vortex in the body of the cyclone. The flow pattern in hydrocyclones, or cyclones in general, is characterized by two vortices: one that moves down towards the bottom outlet along the wall, leaving the cyclone as the underflow, and one which moves in the opposite direction in the center, leaving as the overflow. Denser fluids will migrate towards the wall due to the centrifugal force while the less dense material will move towards the inner axis and get caught in the inner vortex. In the case of an oil and water mixture, the oil, which is of lesser density than water, will move towards the inner vortex and exit through the top outlet while the water will exit through the bottom outlet.

The concept of hydrocyclone separation is based on gravity separation i.e. the

separation of the fluids is driven by the density difference between the fluids. To illustrate this, an expression for the terminal velocity provides an overview of the forces acting on the droplets and which parameters that plays the main role.

The pressure gradient on a droplet can be expressed by Archimedes principle, i.e. $F_p = \rho_c g V_d$, where V_d is the droplet volume, ρ_c is the density of the continuous phase, and g is the acceleration due to gravity. Applying Archimedes principle to the equation of motion of a droplet, including buoyancy effects, will yield the following expression:

$$m\frac{d\mathbf{v}}{dt} = 3\pi\mu_c D f(\mathbf{u} - \mathbf{v}) + m\mathbf{g} - \rho_c \mathbf{g} V_d \tag{2.1}$$

This can be rewritten to express the terminal velocity which is affected by the buoyant force as presented in 2.2.

$$\mathbf{v}_t = \frac{\mathbf{g} D^2(\rho_d - \rho_c)}{18 f \mu_c} \tag{2.2}$$

where

- $\mathbf{v}_t$ is the terminal settling velocity of a droplet.
- $\mathbf{g}$ is the acceleration due to gravity.
- D is the droplet diameter.
- ρ_d is the density of the droplet.
- f is the drag coefficient.
- μ_c is the viscosity of the continuous phase.

Because hydrocyclones use the centrifugal forces to achieve separation, equation 2.2 must be altered as the gravitational acceleration by centrifugal forces is given by:

$$\mathbf{g} = \omega^2 r \tag{2.3}$$

In this equation ω is the angular velocity and r is the radius of the droplet path.

A combination of equation 2.2 and 2.3 provides an expression for the terminal velocity for an oil droplet affected by the centrifugal forces in a hydrocyclone as shown in equation 2.4 page 9.

$$\mathbf{v}_t = \frac{\omega^2 r D^2 (\rho_d - \rho_c)}{18 f \mu_c} \tag{2.4}$$

The angular velocity and the droplet diameter have the largest impact on the terminal settling velocity and because the angular velocity is easily adjustable, the potential for increasing the terminal settling velocity is large.

The terminal velocity $\mathbf{v}_t$ of a droplet determines the speed of which the oil droplets will move inwards to the center of the hydrocyclone and enter the inner vortex. A higher terminal velocity therefore leads to a higher separation rate and a lower minimum retention time to achieve optimal separation.

2.2 Hydrocyclone efficiency

Several factors play an important role for achieving optimal efficiency of a de-oiling hydrocyclone.

2.2.1 Pressure Drop Ratio

The Pressure Drop Ratio (PDR) is an important factor for ensure optimal hydrocyclone efficiency. The pressure difference between the inlet and overflow is defined as $dP_o = P_i - P_o$, with P_i being the inlet pressure and P_o being the pressure at the overflow. For the underflow, the pressure difference can be defined as $dP_u = P_i - P_u$. With this, a pressure drop ratio can be defined as:

$$PDR = \frac{dP_o}{dP_u} = \frac{P_i - P_o}{P_i - P_u} \tag{2.5}$$

By keeping PDR constant as throughput varies, the flow split remains essentially constant[3]. Increasing PDR means increasing the axial pressure gradient to the overflow, and there is an approximate linear relationship between flow split and PDR[3]. Depending on the hydrocyclone size, the PDR of de-oiling hydrocyclones is typically between to 1.5 and 3.

2.2.2 Flow rate

The flow rate versus efficiency relationship is presented in figure 2.2 page 10 and is typical for de-oiling hydrocyclones. As the flow rate is increased, the centripetal forces increases as well and enhances the separation as shown in equation 2.4 page 9. When the flow rate hits the value of Q_{min}, the efficiency of the hydrocyclone is at its maximum. If the flow rate is increased even further beyond Q_{max}, the efficiency will decrease as the retention time is too low for the separation to finish

before the mixture leaves the hydrocyclone.

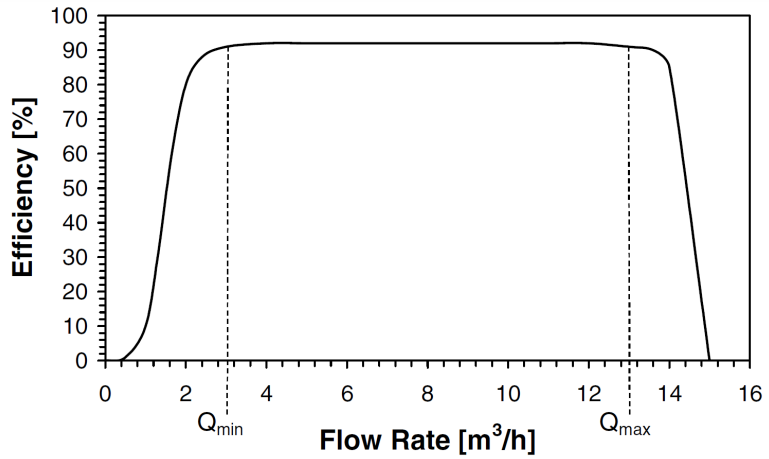

Figure 2.2: Typical hydrocyclone efficiency versus flow rate relationship[3].

2.2.3 Flow split

A minimum flow split is required to ensure a minimum amount of oil will leave through the underflow. The flow split is expressed as Q_o/Q_i, where Q_o is the flow rate at the overflow and Q_i is the flow rate at the inlet. Usually a flow split of 2-3 % is desired, however a flow split of 1 % has proven to give high oil removal, although the minimum flow split required depends on the amount of oil in the mixture.

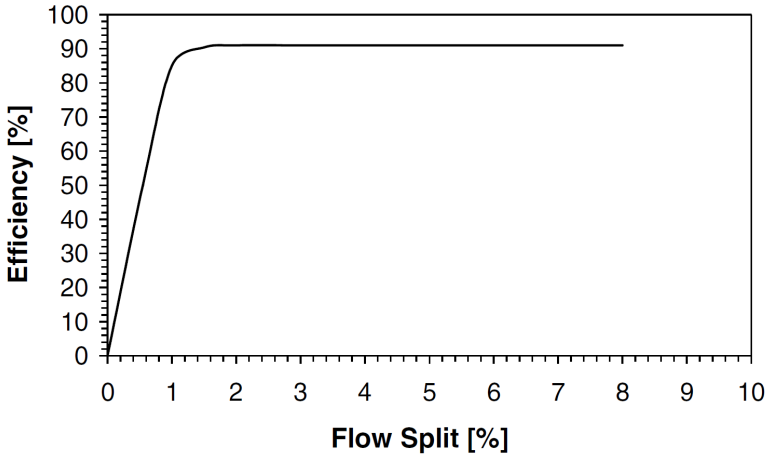

Figure 2.3: Typical hydrocyclone efficiency versus flow split relationship[3].

2.3 Previous CFD work on hydrocyclones

Because hydrocyclones have been used for more than 70 years, many studies have been made on this subject with a wide range of purposes. Newer articles on this subject which also uses computational fluid dynamics in the analysis include:

1) CFD analysis of inlet chamber body profile effects on de-oiling hydrocyclone efficiency[4].

2) Parametric CFD studies on hydrocyclone[5].

3) CFD simulation and experimental validation studies on hydrocyclone[6].

4) Optimizing hydrocyclone design using advanced CFD model[7].

5) CFD simulation of an industrial hydrocyclone with Eulerian-Eulerian approach: A case study[8]

Article 1 analyzed the inlet chamber body profile effects on the efficiency of a de-oiling hydrocyclone. They found that the efficiency can be improved by approximately 8% by using an exponential body shape and the simulations illustrated that recirculating eddies that exist in the upper section prevents inward radial flow and therefore reduces the efficiency. It was shown that the inlet chamber shape affects the size of these eddies.

Article 2 is a parametric CFD study on hydrocyclones which revealed that the cyclone cut size increases with the following changes:

- Increase in vortex finder diameter.
- Decrease in the spigot diameter.
- Decrease in the inlet velocity of the fluid.
- Decrease in the viscosity of the fluid.

Article 3 is also a parametric CFD study which revealed the following:

- Decrease in the spigot opening increased the upward vertical velocity of water more compared to a decrease in the downward vertical velocity.
- Increasing the inlet pressure increased the axial velocities of water in both directions and increased the mass flow rates through the hydrocyclone.
- Increasing the inlet pressure increased the static pressure differential pressure along the radius within the cyclone body, hence more water split into the overflow.

- Increasing the inlet pressure also increased the tangential velocities and reduced the cyclone cut size.

Article 4 used an in-house CFD code as a development tool to eliminate the need to fabricate and test each new design concept.

Article 5 is a standard case study of a CFD simulation of a hydrocyclone which came up with the following results:

- Decreasing inlet solid percentage and increasing the pulp inlet velocity improved the efficiency of the hydrocyclone.
- Decreasing the apex diameter caused an increase in the hydrocyclone.

In order to reduce the amount of work required regarding the setup of the CFD model, these articles have been used as inspiration and a base structure for the final CFD model.

As supplement to these articles, a study has been made on the performance of a deoiling hydrocyclone during variable flow rates[3]. This study does not contain any CFD model, but is a description of experimental investigations and hydrocyclone efficiency during transient flow rates. It includes valuable information regarding hydrocyclone operation with different flow rates and is therefore used as inspiration for this project.

Some remaining work is on the subject of evaluating the flow field if running the hydrocyclone of several flow rates and hydrocyclone efficiencies which is the reason for this project.

3 Modelling Framework

This chapter covers the theory behind the CFD model used to analyze the hydrocyclone along with the decisions and assumptions made during the process.

3.1 What is CFD?

CFD is an abbreviation for Computational Fluid Dynamics and is a finite volume method used for analyzing and solving problems within the field of fluid mechanics. CFD uses numerical methods and algorithms to create simulations of fluid flows, heat transfer, and chemical reactions. This tool has countless applications such as:

- Aerodynamics
- Turbomachinery
- Chemical processes
- Fluid flow
- Acoustics

During the last 40 years, computer aided engineering has become much more common in every day engineering and has therefore resulted in an explosion in CFD codes, even though the governing equations for fluid flow that is being used has been known for more than a hundred years. CFD codes have been developed, improved, and altered in many ways and today there are a number of codes available as both open source, such as OpenFOAM and SU2, and commercial codes, such as Fluent, COMSOL, and Star-CMM+.

The CFD code used in this project is ANSYS Fluent, which is a code used by thousands of companies worldwide as it is one of the most comprehensive software packages for CFD modelling available today.

3.2 Governing equations

The governing equations of fluid flow represent mathematical statements of the conservation laws of physics[9]. These laws are:

- The conservation of mass
- Newton's 2^{nd} law

- The first law of thermodynamics

The conservation of mass is described by the continuity equation, Newton's 2^{nd} law by a momentum equation, and the first law of thermodynamics is described by an energy equation. Because there is no heat transfer of interest in this project, the third conservation law is not being considered further.

Each of these equations are being presented in the form to fit the multiphase mixture model, which is being used to model the multiphase flow in this project. The mixture model is an Eulerian model which can be used to model fluid flow with two or more phases by using a transport equation for each additional phase.

3.2.1 The continuity equation

The continuity equation expresses the mass balance i.e. the balance of the outflow and inflow for a given volume element is zero at any time. For an incompressible flow, the continuity equation is defined in equation 3.1.

$$\nabla \cdot \overrightarrow{u}_m = 0 \tag{3.1}$$

where $\overrightarrow{u}_m$ is the mixture velocity given by:

$$\overrightarrow{u}_m = \sum_{k=1}^{n} \frac{\alpha_k \rho_k}{\rho_m} v_k \tag{3.2}$$

where α_k is the volume fraction and $\overrightarrow{v}_k$ is the velocity of a phase k. ρ_k and ρ_m is density for the phase, k, and for the mixture, respectively. The mixture density is defined by:

$$\rho_m = \sum_{k=1}^{n} \alpha_k \rho_k \tag{3.3}$$

3.2.2 The momentum equation

The momentum equation describes the pressure and velocity in a volume element. Depending on the model used for simulating the flow and if the flow is single- or multiphase, the momentum equation is described differently. Here, the mixture model is used for which the momentum equation can be obtained by summing the individual momentum equations for all phases while using the mixture density and mixture velocity. This momentum equation can be expressed as in equation 3.4 page 15[10][11].

$$\underbrace{\frac{\partial}{\partial t}\left(\rho_m \overrightarrow{u}_m\right)}_{\substack{\text{accumulation}\\ \text{term}}} + \underbrace{\nabla \cdot \left(\rho_m \overrightarrow{u}_m \overrightarrow{u}_m\right)}_{\substack{\text{convection}\\ \text{term}}} = \tag{3.4}$$

$$\underbrace{-\nabla P}_{\substack{\text{pressure}\\ \text{gradient}}} + \underbrace{\nabla \cdot \left[\left(\mu_m + \mu_t\right)\left(\nabla \overrightarrow{u}_m + \nabla \overrightarrow{u}_m^T\right)\right]}_{\substack{\text{laminar stress and Reynolds stress}\\ \text{term}}} +$$

$$\underbrace{\rho_m \overrightarrow{g}}_{\substack{\text{Gravity}\\ \text{term}}} + \underbrace{\rho_k \nabla \cdot \left(\sum_{k=1}^{n} a_k \overrightarrow{u}_{dr,k} \overrightarrow{u}_{dr,k}\right)}_{\substack{\text{Diffusion stress}\\ \text{term}}}$$

where μ_m is the mixture viscosity and $\overrightarrow{u}_{dr,k}$ is the drift velocity of the secondary phase, k. The mixture viscosity and drift velocity is given by:

$$\mu_m = \sum_{k=1}^{n} \alpha_k \mu_k \tag{3.5}$$

$$\overrightarrow{u}_{dr,k} = \overrightarrow{u}_k - \overrightarrow{u}_m \tag{3.6}$$

μ_t is the turbulent viscosity which represents the effect of turbulence on the average flow field. This parameter is modeled using equation 3.7.

$$\mu_t = \rho C_\mu \frac{k^2}{\varepsilon} \tag{3.7}$$

Here, k is the turbulent kinetic energy, ε is the dissipation rate, and C_μ is a constant that depends on the turbulence model it is applied to. For the standard k-ε model this constant is 0.09, while it is 0.0845 for the k-ε RNG model.

Equation 3.4 are also known as the Reynolds Averaged Navier-Stokes (RANS) equations, which are a set of momentum equations that are modified to handle turbulent flows. The idea behind the RANS equations is to make use of Reynolds decompositioning, ensemble averaging, and the Buossinesq approximation, the latter being the basis for the turbulent viscosity.

Having the continuity equation and the three momentum equations yields a closure problem as there is 10 unknowns, but only four equations; this is where the turbulence models comes into play.

3.2.3 The RNG k-ε model

The eddy viscosity approach for solving the closure problem was proposed by Prandtl, where the Reynolds stress terms are thought to behave like viscous terms and a turbulent viscosity[12].

Several types of models were developed to determine this eddy viscosity, some of the most simple models being zero-equation models, where simple algebraic relations are used to solve this parameter. A more complex model set is the two-equation models, where e.g. the k-ε and the k-ω models appear. For this project, the two-equation RNG k-ε model is used, which are defined as the two equations presented in 3.8 and 3.9.

$$\underbrace{\rho_m \frac{\partial k}{\partial t}}_{\substack{\text{accumulation}\\ \text{term}}} + \underbrace{\rho_m \nabla \left(k \overrightarrow{u}_m\right)}_{\substack{\text{convection}\\ \text{term}}} = \underbrace{\nabla \cdot \left(a_k \mu_t \left(\nabla k\right)\right)}_{\substack{\text{diffusion}\\ \text{term}}} + \underbrace{G_k}_{\substack{\text{production}\\ \text{term}}} - \underbrace{\rho\epsilon}_{\substack{\text{dissipation}\\ \text{term}}} \tag{3.8}$$

and

$$\underbrace{\rho_m \frac{\partial \varepsilon}{\partial t}}_{\substack{\text{accumulation}\\ \text{term}}} + \underbrace{\rho_m \nabla \left(\varepsilon \overrightarrow{u}_m\right)}_{\substack{\text{convection}\\ \text{term}}} = \underbrace{\nabla \cdot \left(a_\varepsilon \mu_t \left(\nabla \cdot k\right)\right)}_{\substack{\text{diffusion}\\ \text{term}}} + \underbrace{C_{1\varepsilon} \frac{\varepsilon}{k} G_k}_{\substack{\text{production}\\ \text{term}}} - \underbrace{C_{2\varepsilon} \rho \frac{2\varepsilon}{k}}_{\substack{\text{dissipation}\\ \text{term}}} - \underbrace{R_\varepsilon}_{\substack{\text{turbulent viscosity}\\ \text{effects term}}} \tag{3.9}$$

G_k represents the generation of turbulent kinetic energy due to the mean velocity gradients and is defined in equation 3.10.

$$G_k = \mu_t S^2 \tag{3.10}$$

$C_{1\varepsilon}$ and $C_{2\varepsilon}$ are model constants given by 1.42 and 1.68, respectively[11].

The remaining parameters in the transport equations are presented in the below itemization.

- k is the turbulent kinetic energy
- ε is the dissipation rate
- a is the inverse effective Prandtl number
- R_ε accounts for the effects of turbulent viscosity
- S is the modulus of the mean rate-of-strain tensor

3.2.4 Void fraction

The mixture model solves the volume fraction for the secondary phase, p, using the continuity equation for this phase. The volume fraction equation is defined in equation 3.11.

$$\rho_p \frac{\partial a_p}{\partial t} + \rho_p \nabla \cdot \left(a_p \overrightarrow{v}_m\right) = -\rho_p \nabla \cdot \left(a_p \overrightarrow{v}_{dr,p}\right) + \sum_{q=1}^{n} \left(\dot{m}_{qp} - \dot{m}_{pq}\right) \tag{3.11}$$

where $\dot{m}$ is the mass flow of the phases.

3.3 Boundary conditions

The boundary conditions contain some of the most critical factors that have to be adjusted in order to achieve proper results in any CFD model. The boundary conditions must be considered at the inlet, all outlets, and the wall.

3.3.1 Inlet

The hydrocyclone inlet is a velocity inlet. This means that the boundary conditions for this type are used to define the flow velocity along with all relevant properties of the flow. In this case, the velocity magnitude and direction is set to simulate the laboratory setup with varying flow rates. The flow direction will always be in the y-direction, due to the way the geometry is built and simplified for meshing purposes.

Another factor to consider at the velocity inlet is the hydraulic diameter. This parameter is of relevance because the large eddies in the turbulent length scale, l, cannot be larger than the duct. An approximate relationship between l and the size of the duct is given by:

$$l = 0.07L \tag{3.12}$$

L is the relevant dimension of the duct and this can be based on the hydraulic diameter. The hydraulic diameters at the inlet and outlets are therefore defined according to the diameter of the inlet and outlets on the hydrocyclone. If the turbulent length scale is known, the turbulent dissipation rate, ε, can be determined from equation 3.13 page 17[13].

$$\varepsilon = C_{\mu}^{3/4} \frac{k^{3/2}}{l} \tag{3.13}$$

At the inlet, the hydraulic diameter is $D_{H,inlet} = 7.75 \cdot 10^{-3} m$

3.3.2 Outlets

Both outlets are pressure outlets. This type of outlets require an input in form of a gauge pressure. The exact value for these outlets are set to simulate the experiments performed in the laboratory and these pressures' objective in this project is to act as pressure regulating valves that are mounted at the outlet pipes on the hydrocyclone controlling the PDR. The hydraulic diameters are $D_{H,overflow} = 2.50 \cdot 10^{-3} m$ and $D_{H,underflow} = 1.25 \cdot 10^{-2} m$ at the over- and underflow, respectively.

3.3.3 Wall

The boundary conditions near the wall depends on the near wall treatment and wall functions used to model the flow near the wall. To do this, an understanding of the wall boundary layer is necessary.

Near wall treatment

To account for the near wall modeling, it is ideal to increase the number of mesh cells near the wall, to accurately resolve the large gradients. This is costly to do for any numerical computations, so often it is desirable to use wall treatment modeling to account for the wall conditions.

There are mainly two ways to perform the wall treatment. One is to abstain from resolving the viscosity affected inner region, that is the viscous sublayer and the buffer layer, instead wall functions are used to connect the viscosity affected inner region and the fully turbulent region, also known as the log law region. These regions are depicted in figure 3.1.

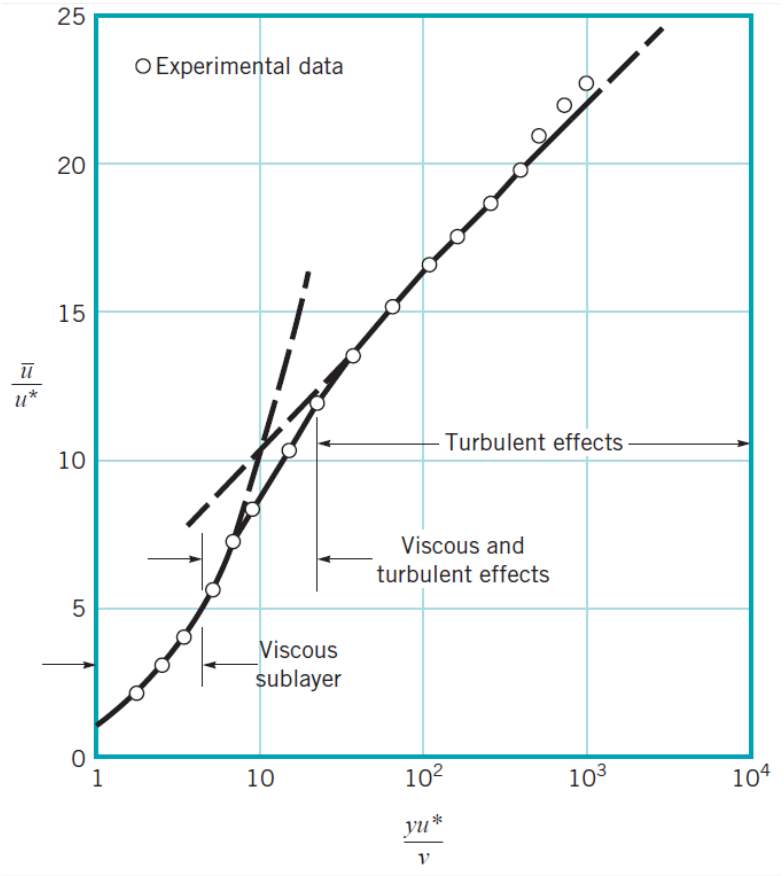

Figure 3.1: The three defined wall regions for turbulent flows[14].

An alternative to the wall functions is the near-wall modeling approach, for which adequate mesh resolution will have to be provided. ANSYS Fluent uses the enhanced wall treatment for near-wall modeling, which is available for the RSM and k-ε models.

Wall functions

ANSYS Fluent provides the following four pre-defined wall functions, with the possibility to apply user-defined wall functions.

- Standard Wall Functions
- Scalable Wall Functions
- Non-Equilibrium Wall Functions
- Enhanced Wall Functions

The use of these wall functions depend on the way the grid is structured close to the wall. A parameter for evaluating this is y^+, which is a dimensionless parameter which can be defined as a dimensionless distance from the wall. y^* is a dimensionless number comparable to the dimensionless y^+ value, and y^* is also proportional to the grid size near the wall[15].

The Scalable Wall Functions will produce the same results as the Standard Wall Functions for $y^* > 11$, which is the case for this project. The Enhanced Wall functions requires even lower y^+ values, $3 - 10$, to be appropriate while Non-Equilibrium Wall Functions not will be suitable either. As a result of this the Standard Wall functions is chosen for this project. The standard wall functions used in ANSYS Fluent is based on the work of Launder and Spalding[16], i.e. using the log-law to describe momentum. However the standard wall functions deteriorate when the dimensionless distance of y^* is below 15.

3.4 Computational procedure

A proper computational procedure is set up to solve for the specific problem that is being dealt with. It is necessary to select the discretization scheme and a solver for the pressure-velocity coupling to reach adequate results.

3.4.1 Discretization

When solving the differential equations, some sort of discretization is required to make them suitable for numerical evaluation. There are several different schemes available for this purpose.

- First-Order Upwind Scheme
- Second-Order Upwind Scheme
- QUICK
- Third-Order MUSCL Scheme

Among these the QUICK discretization scheme stands out as suitable for this project. The QUICK scheme uses a weighted average of 2^{nd} order and central difference, it has increased accuracy for swirling flows[16], and it will converge faster than other 3^{rd} order accurate schemes if the mesh is of a high quality. QUICK is used as the discretization scheme for all but the pressure, where the scheme PRESTO! is used.

PRESTO! is an abbreviation for Pressure Staggering Option and is reported as good for high speed swirling flows[16] and is therefore the preferred choice for a hydrocyclone modeling.

3.4.2 Pressure-velocity coupling

The discretized form of the momentum equations have a linear dependence of velocity on pressure and pressure on velocity. ANSYS Fluent provides several pressure-velocity coupling algorithms to solve this, e.g. SIMPLE, SIMPLEC, and PISO.

For the transient simulations the PISO algorithm is used. PISO is an abbreviation for Pressure Implicit with Splitting of Operators and it is a calculation procedure originally intended for non-iterative computation of unsteady flows. It is highly recommended by ANSYS for all transient flows. PISO is a part of the SIMPLE family of algorithms and it is based on the higher degree of approximation relation between corrections for pressure and velocity.

For the steady-state simulations the SIMPLEC algorithm is used. This algorithm is the Consistent version of SIMPLE, which is short for Semi-Implicit Method for Pressure-Linked equations and it is found to converge faster than SIMPLE and the cost per iteration is approximately the same.

The initial flow field and pressure distribution in the domain have to be guessed. The momentum and continuity equations have to be solved by iterating as they are coupled and non-linear. Based on this assumption the momentum equations are solved for the velocities. To satisfy the discrete continuity equation corrections is done to the velocities and pressure. The SIMPLE algorithm also corrects velocities and pressure to satisfy the momentum. The principle of this algorithm can be seen in equations 3.14 and 3.15 page 21.

$$u = u^* + u' \tag{3.14}$$

$$p = p^* + p' \tag{3.15}$$

where

- u and p are the variables to be solved
- u^* and p^* are the guessed values
- u' and p' are the corrected values

The SIMPLE method is iterative and the calculations needs to be done sequentially. The SIMPLEC follows the same steps as the SIMPLE algorithm, however the momentum equations are manipulated so that the SIMPLEC velocity equations omit terms that are less significant than those in SIMPLE[9].

The SIMPLE and PISO algorithm schemes can be found in appendix D and E, respectively.

3.4.3 Initialization and convergence criteria

Before starting any CFD simulation, the solution must be initialized. The standard initialization is used, which initializes the flow field in the entire domain. This allows for set initial values to be used in the calculation.

The convergence criteria can be almost any parameter desired by the user. Often the residual plot is used for this purpose where either a full convergence is achieved or a suitable low error between the iterations is present. In this case, the inlet pressure and outlet densities will be measured during the simulation and when the values has reached a steady value, the flow is considered to be in steady-state and the simulation is finished.

3.5 Discussion and choice of models

This section will discuss the choice of models used to model the turbulence and the multiphase flow as well as the oil droplet size.

3.5.1 Turbulence model

The turbulence model chosen for this case is, as already presented in section 3.2.3, the RNG k-ε model. This model is one of three k-ε models, which are the most

common turbulence model type used in the industrial sector. The choice of the RNG k-ε model is based previous work on turbulence models where it has been reported as useful[6][8].

This model has a set of refinements to the standard k-ε model:

- An additional term in the ε equation that improves accuracy for rapidly strained flows.
- The effect of swirl on turbulence is included in the RNG model.
- Provides an analytical formula for turbulent Prandtl numbers as oppose to the standard model that uses user-specified constant values.
- Provides an analytically derived formula for effective viscosity that accounts for low-Reynolds number effects. To use this optimally, proper treatment of the near-wall region must be applied.

These refinements are what makes this specific model good for modeling the turbulence in hydrocyclones. Additionally, the k-ε models in general are:

- a very robust set of models
- fairly accurate due to a 40 year development span
- computationally cheap

LES

Large Eddy Simulation (LES) is a model that could have been used for this project. However, the inherent unsteady nature of LES suggests that the computational requirements should be much larger than those of classic turbulence models and twice the power of the Reynolds Stress Model for the same simulation[9].

It is not desired to use such a computational heavy model if sufficient results can be obtained by other models, which is supposed to be possible according to several studies on hydrocyclones[4][5][6][7].

3.5.2 Multiphase model

ANSYS Fluent models multiphase flows using the Euler-Euler approach, meaning that the different phases are treated mathematically as interpenetrating continua[11]. The following three Euler-Euler multiphase models are available, which each should be used for specific applications due to the way they are handling the phases:

- The Volume of Fluid model
- The Eulerian model
- The Mixture model

The Volume of Fluid model is designed for two or mode immiscible fluids where the position of the interface between the fluids is of interest[11]. Flow applications for this model include free-surface flows, the motion of large bubbles in a liquid, and the transient tracking of any liquid-gas interface.

The Eulerian model is the most complex multiphase model available in this software. This model solves a set of n momentum and continuity equations for each phase and the coupling is achieved through the pressure and interphase coefficients. Applications include bubble columns, particle suspension, and fluidized beds.

The Mixture model is defined for two or more phases and it solves for the mixture momentum equation and prescribes relative velocities to describe the dispersed flow. Applications for the mixture model includes bubbly flows, sedimentations, and cyclone separation.

The mixture model is chosen for this project as it is recommended for modeling of cyclone separation. When applying this model, the number of Eulerian phases must be set to two, i.e. the water phase and the oil phase in the hydrocyclone. Calculation of slip velocities and large body forces is included in this model in order to make the model appear as close to reality as possible. The large body forces includes gravity and surface tension forces which is also desired to include in the model, as the extra body force correction terms allows for the flow to achieve a realistic pressure field very early in the iteration process[11]. Another benefit of including the large body forces is that the solution will be more robust.

3.5.3 Droplet size

The oil-water mixture used for the experiments has not been through a separator before entering the hydrocyclone. In a real system in operation with a de-oiling hydrocyclone, the mixture will flow through a separation tank beforehand which will sort out all the larger particles. After the separator, only very small particles would be transfered with the water towards the hydrocyclone. The oil used in this experiment is motor oil which comes directly from the barrel and into the water towards the hydrocyclone.

To determine the average oil droplet size, an oil droplet size study has been made where particle sizes tested in the CFD model until the mixture density at the overflow matched the experiments. The relevant data from this study can be found in appendix C, and the average droplet size has be determined to be roughly 400μm, which is used for the CFD simulations.

This parameter becomes important for the mixture model in the way the slip velocity is calculated. The slip velocity is given by equation 3.16.

$$\overrightarrow{v}_{pq} = \frac{\tau_p}{f}\frac{\rho_p - \rho_m}{\rho_p}\overrightarrow{a} \tag{3.16}$$

where τ_p is the droplet retention time given as:

$$\tau_p = \frac{\rho_p D_p^2}{18\mu_q} \tag{3.17}$$

This retention time is of same form as equation 2.2 page 9 which clearly states a relationship between the retention time and terminal velocity.

4 Case setup

This chapter goes through the meshing of the geometry with the simplifications applied and the mesh quality analysis.

4.1 Presentation of geometry

A CAD model of the hydrocyclone was provided at the beginning of the project. The hydrocyclone itself is the hollow volume between two casing parts and is presented in figure 4.1.

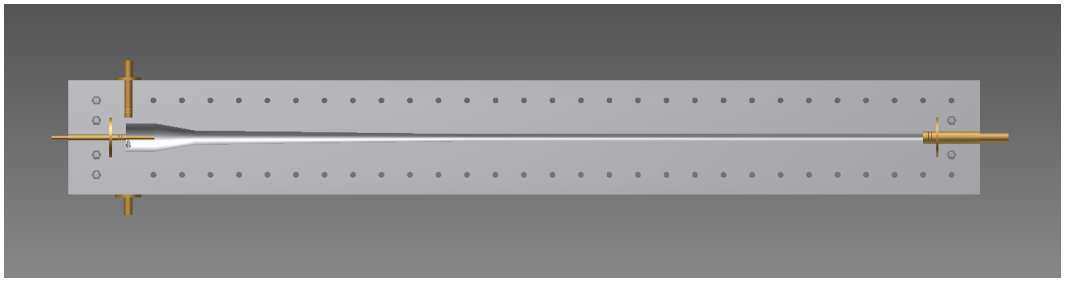

Figure 4.1: The hydrocyclone cut in half, revealing the inner volume.

In order to mesh this geometry, the software CUBIT is used. CUBIT is a full-feature software toolkit for robust generation of two- and three-dimensional grids and geometry preparation. The main goal of CUBIT is to reduce the time it takes to generate meshes and in particular large hex meshes of complicated assemblies[17]. This software is chosen for easing the generation of a structured hex mesh throughout the entire hydrocyclone.

Using CUBIT, the inner volume is extracted from the CAD file and the result of this is presented in figure 4.2:

Figure 4.2: The extracted inner volume of the hydrocyclone.

4.2 Simplifications

Several simplifications were made to the geometry in order to simplify the meshing process. Consider figure 4.3 and 4.4, page 26, where the geometry is presented before and after simplification, respectively.

Initially, two parts of the hydrocyclone was planned to be simplified. The hydro-

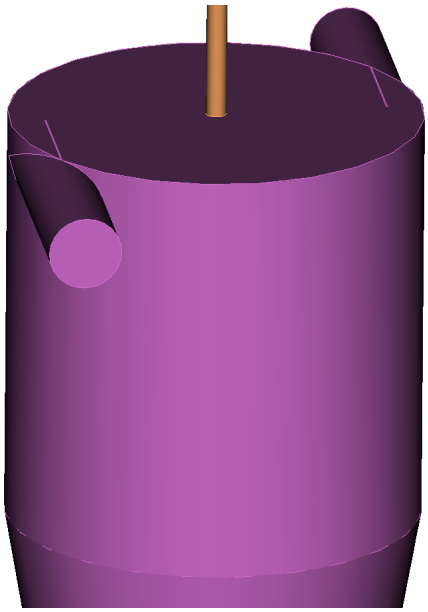

Figure 4.3: Before simplification.

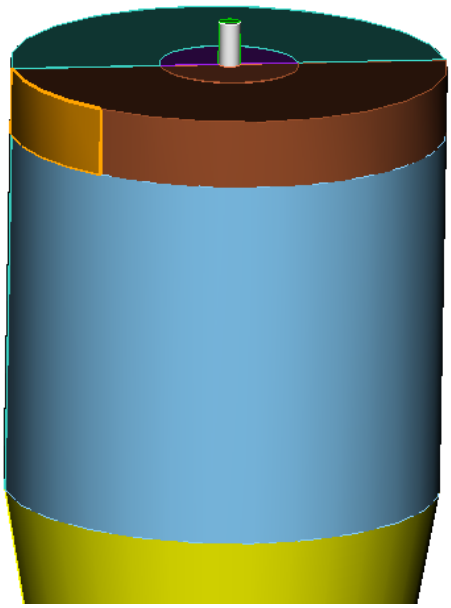

Figure 4.4: After simplification.

cyclone is designed with two inlets in order to enhance the swirl and separation, however, these are reduced to only one inlet in the final geometry.

The other simplification has been made on the overflow outlet pipe, which in the geometry is relatively long and require too many cells for its purpose. This piece of the hydrocyclone does not contain any specific phenomena of interest; only the outlet composition, pressure, and flow rate is of interest. Therefore this outlet is shortened as seen on figure 4.4.

Meshing this geometry has been the source of many issues due to the inlet. At first, the plan was to use a tetrahedral mesh for the inlet pipe and switch to the structured hex mesh right after the inlet. The source of these issues had their root in the skewness and quality of a mesh where this inlet pipe would merge with the rest of the cyclone due to the sharp edges on the merging areas as seen on figure 4.5:

Figure 4.5: The inlet pipe to the hydrocyclone.

Therefore the geometry has been stripped completely for an inlet pipe and a new plane to suit the purpose of the inlet pipe has been created. This plane is shown in orange on figure 4.4 page 26 and it has been designed to cover the same area as the pipe would have. To account for this, the inlet flow will be set in the y-direction in ANSYS Fluent to ensure a correct flow direction for the CFD model.

4.3 Meshing strategy

In figure 4.6 the entire hydrocyclone mesh is shown.

Figure 4.6: The fully meshed hydrocyclone.

Because the mesh contains such a large amount of cells, the hydrocyclone with mesh is broken down in to more pieces to better depict the mesh used for each section.

It is desired to have a full hexagonal mesh in the entire model with the inner part of the model containing a more dense mesh. The reason for a creating a more dense mesh in the center of the hydrocyclone, is due to the fact that this is where the inner vortex, bringing the low-density phase to the overflow, is located. In figure 4.7 the top part of the hydrocyclone is shown on the left and the inner part on the right.

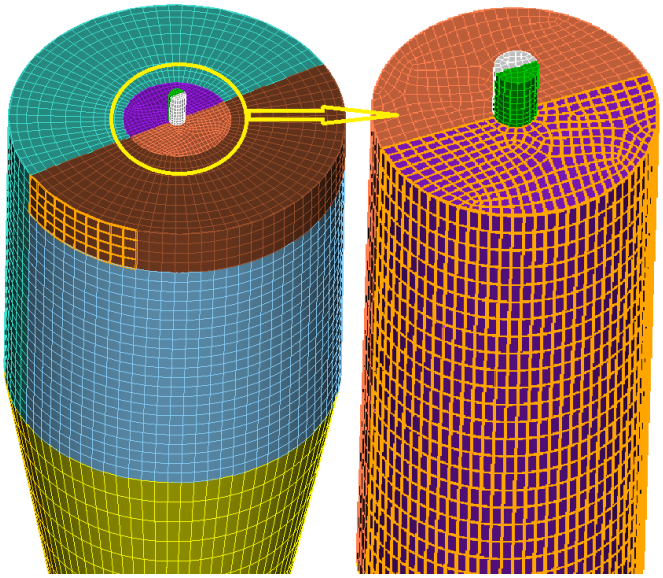

Figure 4.7: The mesh on the upper section (left) and the inner cylinder mesh with overflow outlet (right).

The remaining part of the hydrocyclone is meshed with a simple hexagonal mesh through the entire length of the model as shown in figure 4.8.

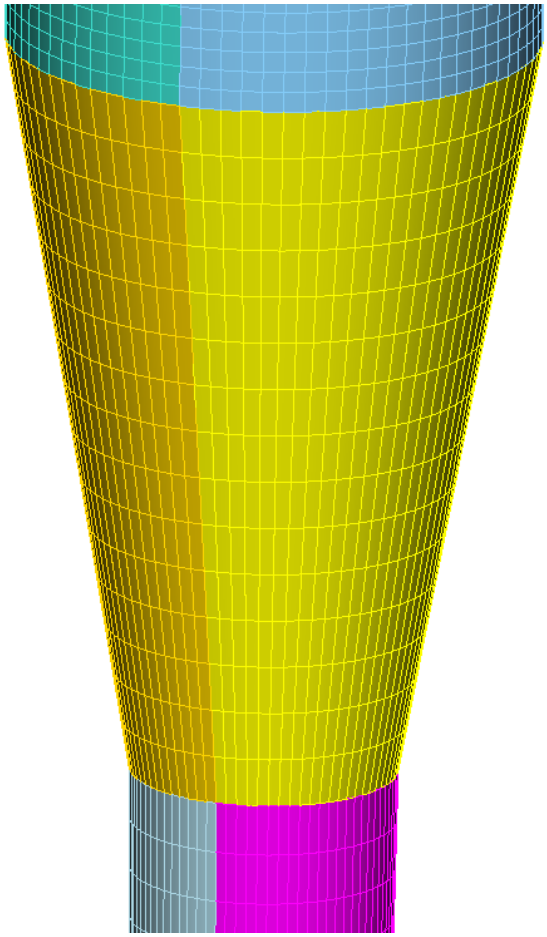

Figure 4.8: The mesh on the upper, middle, and lower section.

4.4 Mesh quality

4.4.1 Aspect ratio

The aspect ratio is the ratio between the longest and shortest side of an element. This describes how compressed an element is and the maximum acceptable range of the aspect ratio is between 20 and 100 in regions of interest while an aspect ratio of 1 is perfect. The minimum, maximum, and average aspect ratio for this mesh is listed in the below itemization.

- Minimum: 1.021
- Maximum: 16.9

- Average: 4.695

From this it can be concluded that the aspect ratio is in full compliance with the best practice guidelines from ERCOFTAC[18].

4.4.2 Skewness

If the mesh contains highly skewed elements, it might prevent the simulation from converging. The skewness is calculated as shown in equation 4.1 for a quadrilateral cell:

$$Skewness = max\left[\frac{\theta_{max} - 90}{90}, \frac{90 - \theta_{min}}{90}\right] \tag{4.1}$$

The range and quality of skewness is explained in the table 4.1.

Q_{EAS}	Quality
$Q_{EAS} = 0.00$	Perfect
$0.00 < Q_{EAS} < 0.25$	Excellent
$0.25 < Q_{EAS} < 0.50$	Good
$0.50 < Q_{EAS} < 0.75$	Fair
$0.75 < Q_{EAS} < 0.90$	Poor
$0.90 < Q_{EAS} < 1.00$	Very poor
$Q_{EAS} = 1.00$	Degenerate

Table 4.1: Range and quality of skewness[19].

The minimum, maximum, and average skewness for this mesh is listed in the below itemization:

- Minimum: $3.534 \cdot 10^{-16}$
- Maximum: $3.737 \cdot 10^{-1}$
- Average: $6.134 \cdot 10^{-2}$

The mesh of an excellent quality when considering the skewness and is also in compliance with the best practice guidelines from ERCOFTAC[18].

4.5 Grid independence

To ensure that a proper mesh is used for modeling the hydrocyclone, a mesh independence study is performed. In order to do this, a set of meshes have been constructed with different amounts of cells. Each mesh with different size is used for a simulation with the same solution method, scheme, and turbulence model. The analysis is performed for a single phase system and the selected parameters for this study can be seen in table 4.2.

Turbulence model	$k-\varepsilon$, RNG, Standard wall function
Solution algorithm	PISO
Discretization scheme	QUICK
Solver	Incompressible, steady state
Inlet boundary condition	Velocity inlet, 15 m/s
Outlet boundary conditions	Pressure outlet, 0 Pa

Table 4.2: Selected solution parameters for the mesh independency study.

The parameter used for the mesh independency study is the pressure at the inlet, with the pressures at the outlets being zero. The results of the mesh independency analysis is plotted in figure 4.9.

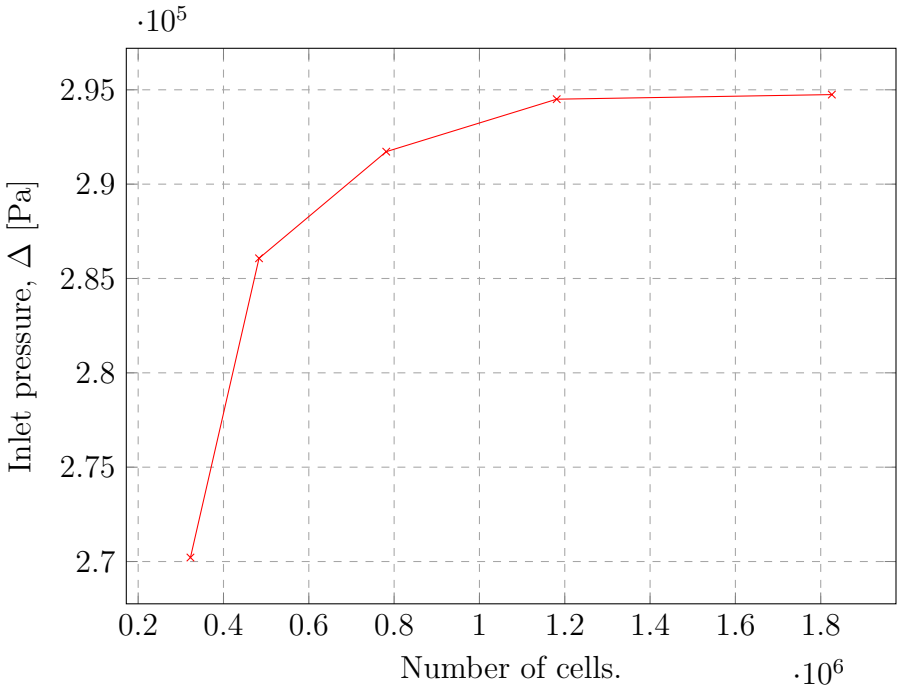

Figure 4.9: Plot of the results from the mesh independence study.

Using these results it is possible to see the mesh which will take the least computational power and still provide an accurate result. Therefore the mesh with $1.2 \cdot 10^6$ cells are chosen for further modeling.

4.6 y-plus

For this project the Standard Wall Functions are used as described in section 3.3.3 page 18. Usually, this requires the y^+ values to be between 30 and 300. The y^+ values calculated by Fluent for this mesh can be seen in figure 4.10.

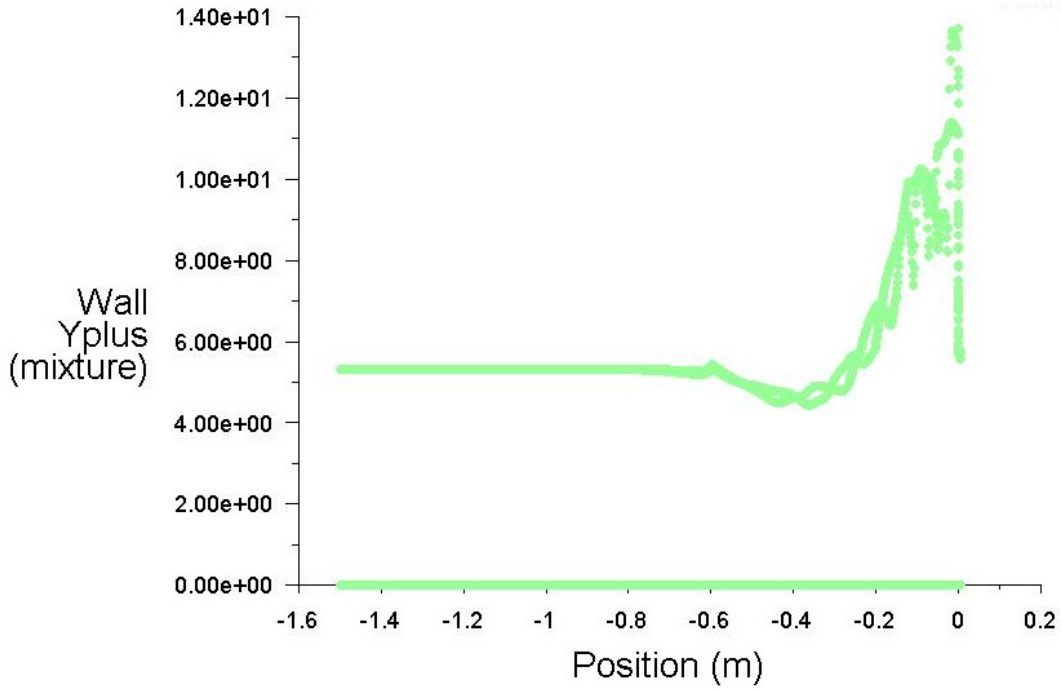

Figure 4.10: The y^+ values through the hydrocyclone.

The figure makes it very clear that the y^+ values are too low. Possible consequences of the y^+ values being too low can be a decrease in the total pressure drop across the hydrocyclone due to a misinterpretation of the wall friction. Because the focus of this project is on the swirl and the interaction between the two vortices, the flow at the walls of the hydrocyclone is not great interest. As a result of this, it is decided to stick with this mesh.

5 Validation experiment

5.1 Purpose of the validation experiment

The purpose of the experiment is to make a validation case to compare with the CFD simulation. For comparison and validation of the CFD model, the mixture density in the overflow will be determined as well as the inlet pressure.

5.2 Materials and equipment

The following materials are used:

- SAE 30 mineral oil from *ardeca Lubricants*
- Water

The properties for the oil is presented in table 5.1:

	Density $\frac{kg}{m^3}$	**Viscosity** $\frac{kg}{ms}$
Water	998.2	$1.003 \cdot 10^{-3}$
Oil	826	0.31

Table 5.1: Density and viscosity of oil and water at 25 degree C.

The density of the oil has been determined experimentally, as the data sheet available for the oil was not sufficient. See appendix B for details regarding the determination of the oil density.

The following equipment are used along with the P&ID notations, as presented in 5.1 page 33.

- Three ABB 10DX4311 Magnetic Flowmeters, MFM
- A CMFS010M300N0ANACZZ Coriolis Flowmeter, CFM
- A TTFM 1.0 Transit Time ultrasound flowmeter, UFM
- Siemens SITRANS P200 Pressure transmitters, PT
- Water pump, WP
- Oil pump, OP

- Oil container, HE2
- Water container, HE3
- Buffer tank, HE4
- Mixer
- Control valves, CV
- Shut-off valves, HCV
- Computer for data logging and system control
- Canon EOS 600D camera

The P&I diagram of the entire test setup can be found in appendix A and a simplified version of this is presented in figure 5.1. A photograph of the hydrocyclone in the laboratory is presented in figure 5.2.

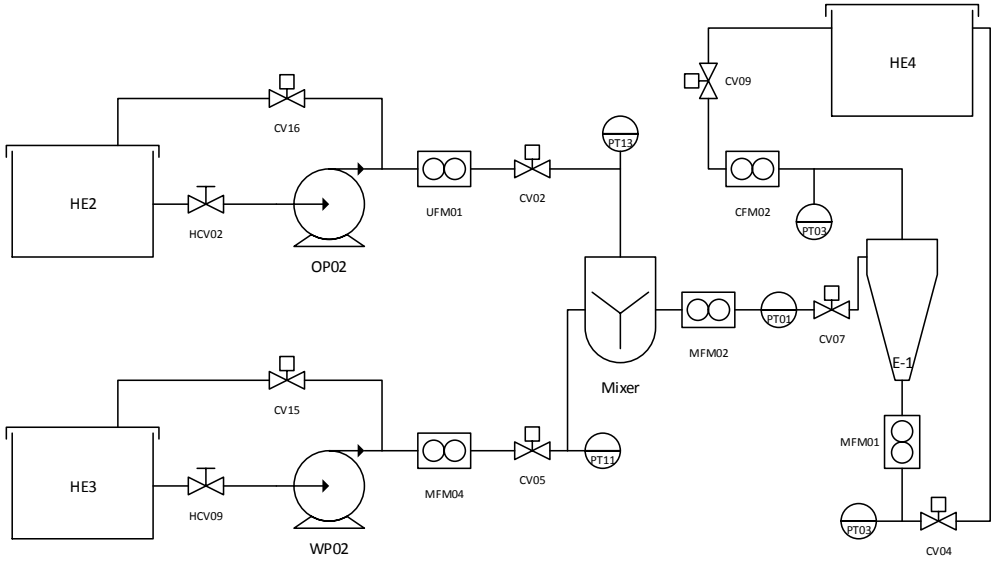

Figure 5.1: Simplified P&I diagram of the hydrocyclone test setup.

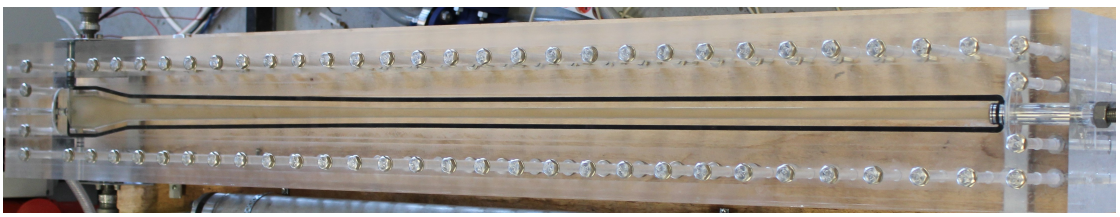

Figure 5.2: Photograph of the hydrocyclone.

5.3 Methods

1) Control valves CV07, CV09, CV10, CV04, and CV05 are fully opened to allow fluid flow to into and out of the hydrocyclone.

2) Control valves CV02 and CV16 are 50% open to allow for a return flow for easing the low oil flow rate required to mix with the water flow.

3) Control CV15 is fully closed to achieve the maximum flow rate towards the hydrocyclone.

4) The water pump speed is set to 100% to achieve maximum flow rate of approximately 0.7 L/s.

5) The oil pump is set to match a mass flow rate of 5% of 0.7 L/s. This cannot be done directly, so the oil pump speed is adjusted until a decent flow rate is reached.

6) 12 tests of 5 minutes is run.

   - Six tests to ensure correct setup and a complete mix of oil and water entering the hydrocyclone.
   - One test to check consistency of results.
   - Five tests for documenting the flow and data acquisition.

7) The flow inside the hydrocyclone is recorded using the Canon EOS 600D camera.

8) The data is for all flow meters and pressure transmitters is logged automatically in MATLAB.

5.4 Measuring uncertainty

In the hydrocyclone setup there are several different types of data transmitters used to log the pressure, flow rate, and density on specific positions.

The pressure transmitters are Siemens SITRANS P200 which has a measurement deviation of typically 0.25% and a maximum of 0.5% at 25°C.

The coriolis flowmeter used to measure the flow rate and density in the overflow has a calibration certificate stating that a measuring error of 0.065%.

The magnetic flowmeters are ABB 10DX4311 sensors with a system accuracy of 0.5%.

The ultrasound flowmeter is a TTFM 1.0 Transit Time Flowmeter which has an accuracy of $\pm$ 1%.

5.5 Results and discussion of the experimental data

The flow through the system is mainly controlled by the water pump which is operated by a PID controller. As a result of that, the pump is constantly regulating the pump speed to come as close to a given set point as constant as possible. A pressure transmitter, PT11, is located at the pump outlet and provides a good indication of the operation of the pump. This is depicted in figure 5.3.

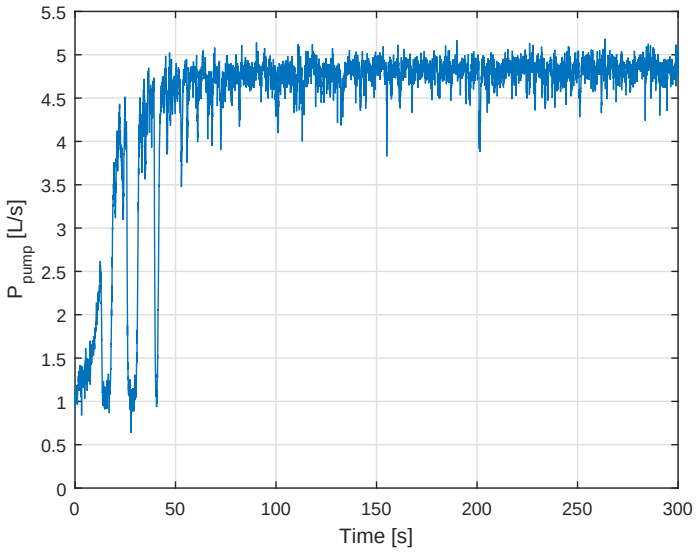

Figure 5.3: The pressure transmitter, PT11, data plot after the water pump.

Over a period of time the flow rates and pressures in the system can be roughly determined by using the mean value. Because the exact values of the pressures and flow rates are not of great importance to reach the conclusion desired, the mean results are considered to be accurate enough for the purpose. The data of interest are the hydrocyclone inlet flow rate and the pressure at the over- and underflow outlets. The acquired data is presented in figure 5.4, page 36, and the values used for the CFD model validation is presented the below itemization:

- Oil fraction: 2.3%
- Hydrocyclone inlet pressure, P_i: 414,000 Pa.

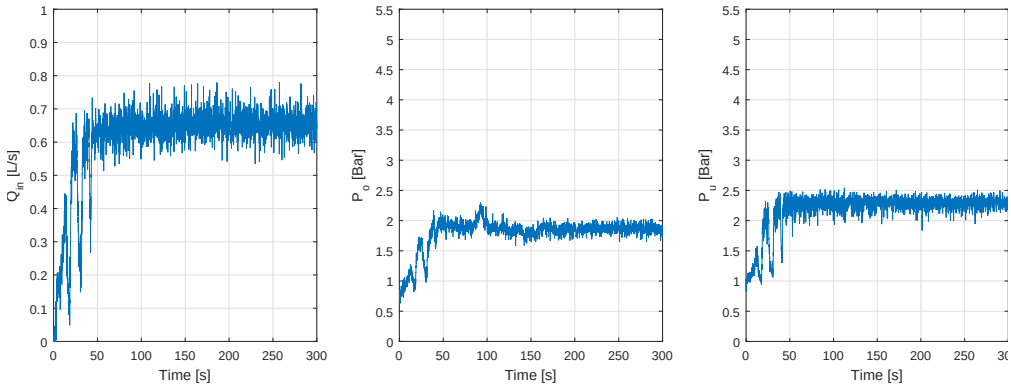

Figure 5.4: The hydrocyclone inlet flow rate with the corresponding over- and underflow pressure.

As oppose to the pressures and flow rates throughout the system, the density is of great importance to determine both the oil fraction in the overflow and the average particle size that is to be used for the CFD model. The density is measured in the coriolis flowmeter, CFM02, and this data is presented in figure 5.5.

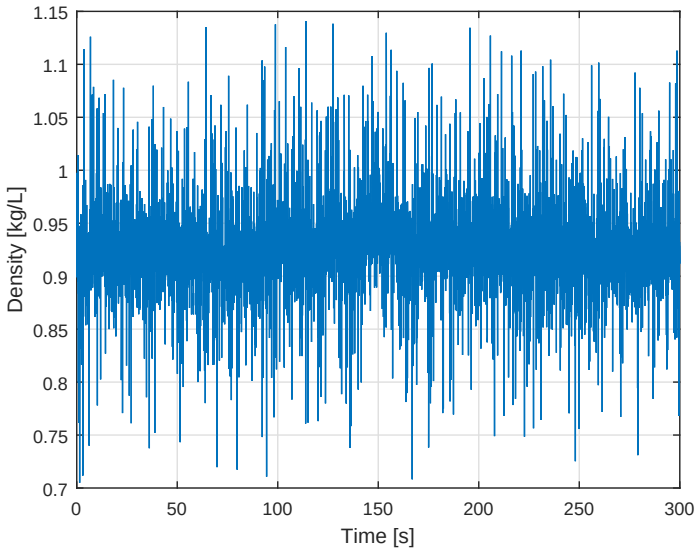

Figure 5.5: The density of the mixture leaving the overflow.

In order to use these results, a histogram with the data has been set up to check if it follows the expected normal distribution.

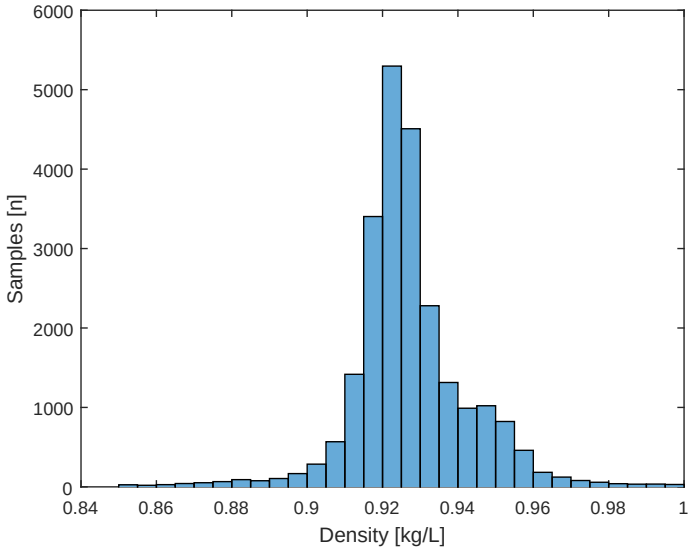

Figure 5.6: The density samples following a normal distribution.

As seen in figure 5.6 there is a deviation from having a smooth normal distribution. When the diagram is broken down into smaller parts to see if one specific period causes this deviation, there is no immediate connection and a deviation of some sort is consistent throughout the entire time period. The reason for this might be caused by the operational patterns of the pumps as presented in figures 5.7 and 5.8.

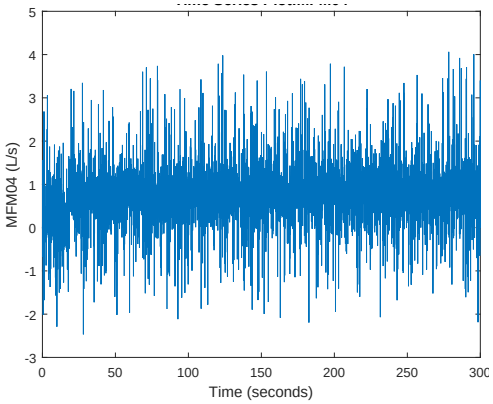

Figure 5.7: Water pump operational pattern.

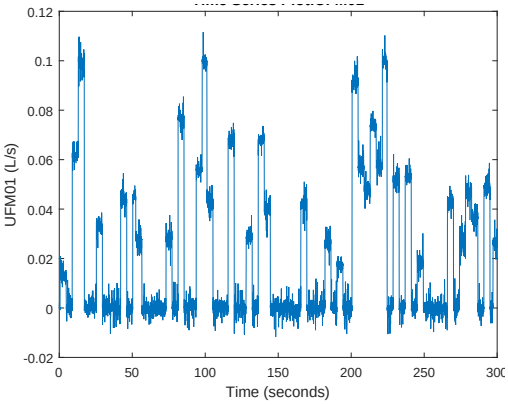

Figure 5.8: Oil pump operational pattern..

As seen in figure 5.7 the water pump is much more consistently running than the oil pump in figure 5.8, which can lead to bursts of higher water flow at the oil pump down time, hence a higher measured density in the overflow.

This data is the best possible to achieve with the available laboratory setup, and

the density determined here is therefore used for further computation.

The standard deviation is 0.0215 and the mean is 0.9268 kg/L. Whether this mean is acceptable for further analysis can be determined using a 95% confidence interval as presented in equation 5.1.

$$0.95 = P\left(\overline{X} - 1.96\frac{\sigma}{\sqrt{n}} \leq \mu \leq \overline{X} + 1.96\frac{\sigma}{\sqrt{n}}\right) \tag{5.1}$$

By inserting the standard deviation and the number of samples, the mean density is $0.9268 \pm 2.72 \cdot 10^{-4}$ kg/L.

The mean density of this mixture used for further modeling is therefore 0.9268 kg/L. The overflow being a mixture of oil and water with known densities, the oil fraction can be calculated. The oil and water fractions are determined from:

$$\rho_{mix} = \frac{\rho_{oil} \cdot x_{oil}}{\rho_{water} \cdot x_{water}} \tag{5.2}$$

Thus, the overflow is a mixture of 58% water and 42% oil. The PDR is determined to be 1.19.

6 Case overview

This chapter provides an overview of the cases set up for the CFD simulation.

Two types of cases are set up to provide a proper basis for evaluating the flow field at several flow rates.

1) A validation case

2) Flow field study cases

The validation case consists of an experiment and a CFD simulation with the goal of validating the CFD model by comparing it with the results obtained from the experiment explained in section 5.

The second case will provide the data and visual presentation of the flow field at different flow rates.

6.1 Validation case

The general setup for the validation case is presented in table 6.1:

Turbulence model	$k-\varepsilon$, RNG, Standard wall function
Solution algorithm	PISO
Discretization scheme	QUICK and PRESTO!
Solver	Incompressible, transient

Table 6.1: Selected solution parameters for the validation case.

The input for this specific case is set to match the experiment and is presented in table 6.2:

Inlet boundary condition	$V_{in} = 14.8$ m/s
Overflow outlet boundary condition	$P_o = 188$ kPa
Underflow outlet boundary condition	$P_u = 230$ kPa
Oil droplet diameter	$D_{droplet} = 400\mu$m
Oil fraction	$\alpha = 2.3\%$

Table 6.2: Selected input parameters for the validation case.

6.2 Flow field study cases

The solution parameters for the flow study cases is presented in table 6.3:

Turbulence model	$k-\varepsilon$, RNG, Standard wall function
Solution algorithm	SIMPLEC
Discretization scheme	QUICK and PRESTO!
Solver	Incompressible, steady-state

Table 6.3: Selected solution parameters for the modifying flow rates case.

As oppose to the validation case, a range of flow rates will be simulated in this case. For all flow rates the oil droplet size will be kept at 400μm and the oil fraction will be 5%. The flow rates, Q_{in}, and outlet pressures in the over- and underflow, P_o and P_u will be altered for each simulation aiming for the same PDR for each simulation under different conditions. The inlet flow rates with corresponding pressures for the over- and underflow used for the simulations are presented in table 6.4:

Case #	Q_{in} L/s	V_{in} m/s	P_o kPa	P_u kPa
1	0.4	8.5	116	146
2	0.5	10.6	126	175
3	0.6	12.7	142	212
4	0.7	14.8	184	282
5	0.8	17.0	205	335

Table 6.4: Boundary conditions applied for the flow study cases.

7 CFD Results

In this chapter, the results from the CFD simulations is presented for the validation case and the flow field study cases.

7.1 Validation case

For the validation case, the convergence criteria is the hydrocyclone inlet pressure and the overflow density. In order to reach an acceptable convergence using the residual plot, the duration for each simulation to finish will greatly increase which the time does not allow. The converged solution criteria is presented in table 7.1.

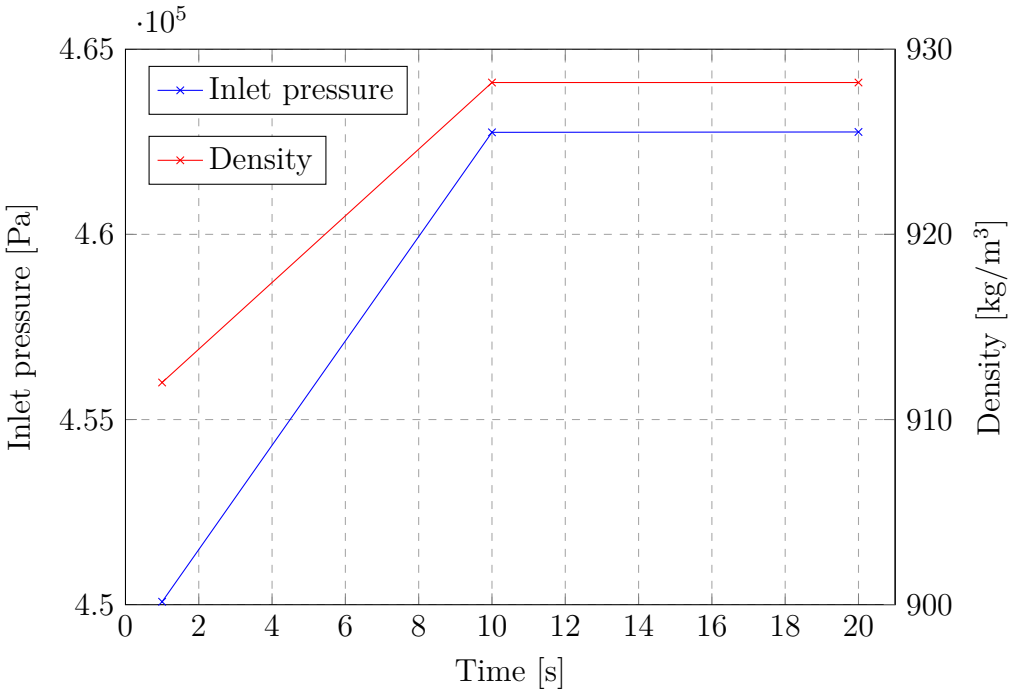

Figure 7.1: The convergence criteria used in the validation case.

After a 20 second simulation, the pressure and density has settled and a steady state solution is assumed to be reached. The data collected at the 20 second mark is used for validating the CFD model against the experiment and the hydrocyclone inlet pressure and density is presented in table 7.1 page 42.

	ρ kg/m^3	P_i kPa	PDR -
Experiment	926.8	414	1.19
CFD model	928.2	463	1.18

Table 7.1: Validation case experimental and CFD data.

7.1.1 Flow field overview

Before going in to detail with the simulations, an overview of the flow inside the hydrocyclone should be considered as each simulation produces a similar pattern. Figure 7.2 depicts the density contour plot through the hydrocyclone and presents a general picture of the oil core.

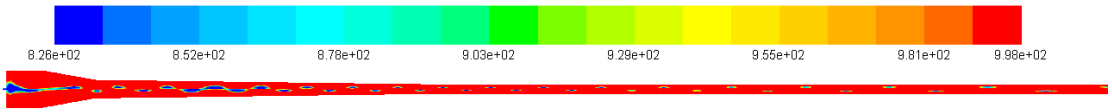

Figure 7.2: Contour plot of the density through the hydrocyclone.

The density in figure 7.2 ranges from 826 kg/m^3 in dark blue to 998 kg/m^3 in red and the oil core is helix shaped due to the vortices inside the hydrocyclone.

A density iso-surface is created which provides a much more clear view of the inner vortex and is presented in figure 7.3 page 43. This iso-surface is created with a density of 870 kg/m^3 to depict the oil flow in the inner vortex. The blue rectangle on the left in the figure is the simplified inlet as discussed in section 4.2 page 25.

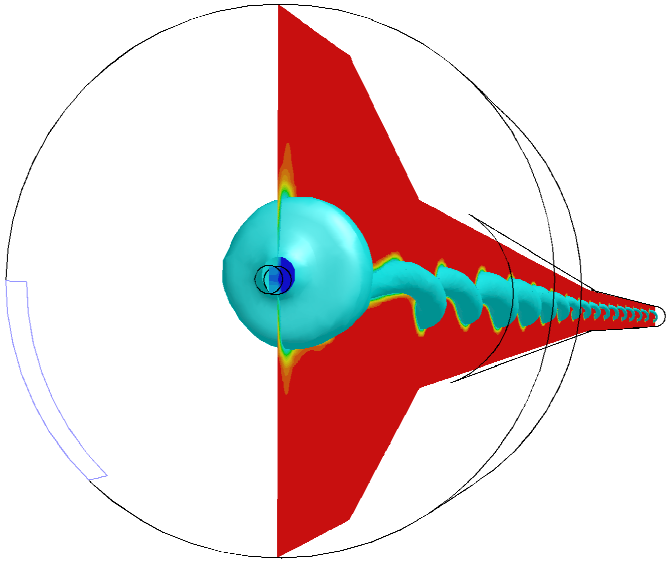

Figure 7.3: Iso-surface with a density of 870 kg/m^3.

7.1.2 Flow field comparison

Photographs is taken of the flow in the hydrocyclone to achieve a basis for validating the CFD model on a flow field perspective. Due to very blurry and unclear images, figure 7.5, 7.6, and 7.7, page 44 to 46, have lines drawn where the oil core is located for clarification.

The first picture presented is figure 7.4 page 44, which shows the top part of the hydrocyclone showing the two inlets and the overflow outlet. This part of the hydrocyclone is depicted with water only because when oil is included, the flow becomes severely blurred and results in zero vision of an oil or air core.

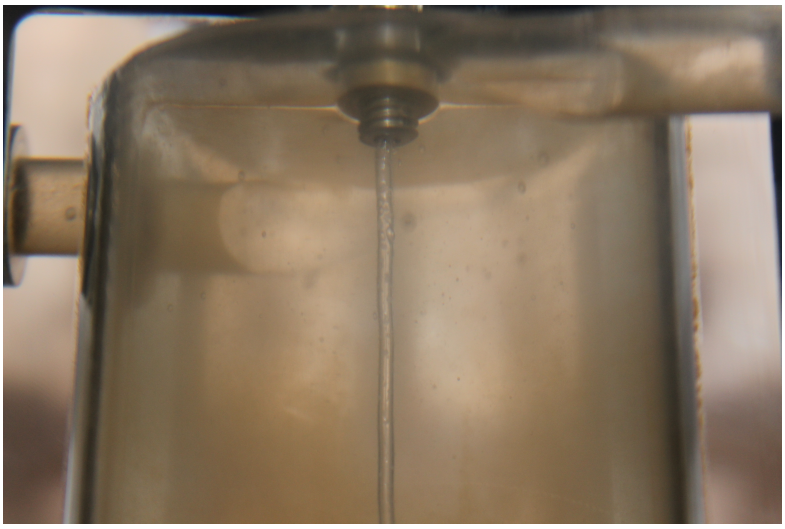

Figure 7.4: Top section of the operating hydrocyclone with water only.

It can be observed that the inner core is relatively narrow and mainly consists of air, as air is the lesser dense fluid which will separate and enter the core when oil is not present. However, air will still be a part of the core when oil is included, but it will not be visible. This can be seen in figure 7.5 where oil is added to the system.

In figure 7.5 oil is added to the system and the hydrocyclone is now separating oil from water. The oil core is relatively clear when looking at the hydrocyclone in real time and it is observed that the oil core vanishes as it enters the wide section of the hydrocyclone, which is presented with water and air in figure 7.4. Figure 7.5 is a combination of a photograph and the density contour plot of the same location in the CFD model.

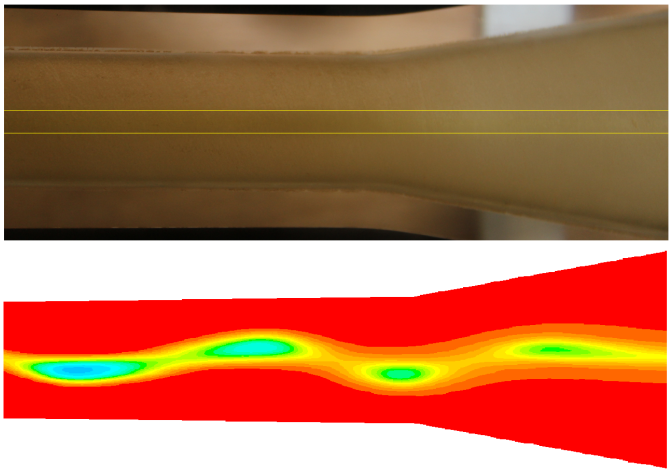

Figure 7.5: The intermediate section.

An immediate observation can be made on the shape of the oil core. The experiment reveals a cylindrical oil core as oppose to the CFD model which shows a helix-shaped oil core. The reason behind this difference can be the fact that the experiment showed an unstable flow field throughout the entire hydrocyclone, which will not be a result of the CFD simulation due to perfect operating conditions. Another issue with matching these pictures is the density distribution which does not match, as the outer vortex should be mainly water and therefore more transparent.

Figure 7.6 is a picture of the flow, half-way down the hydrocyclone. Again, unlike the CFD model, the oil core appears as a stable cylinder.

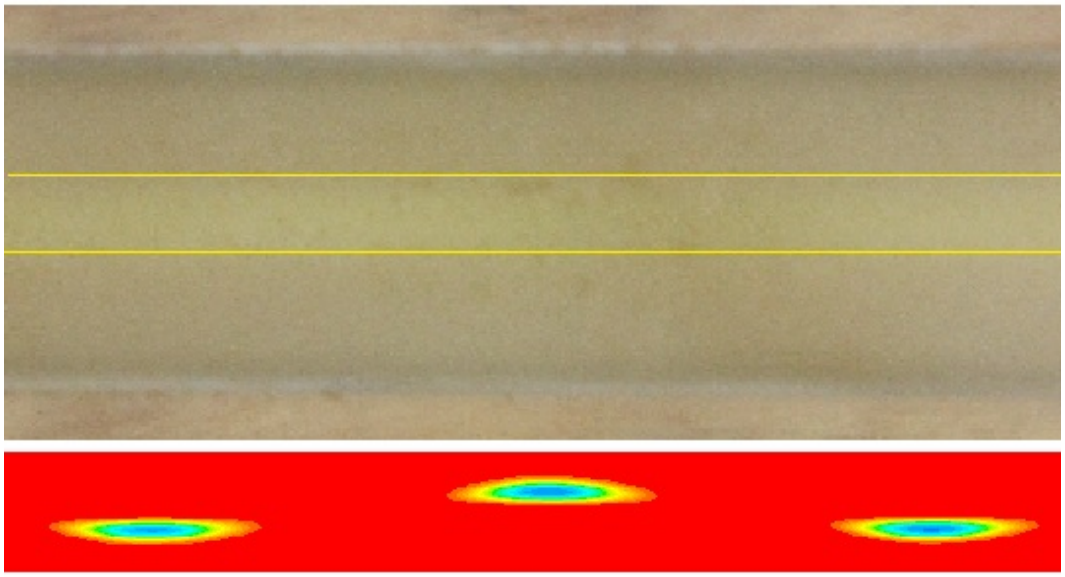

Figure 7.6: Photograph of the middle of the hydrocyclone.

On figure 7.7, page 46, the oil core is much mure unstable than anywhere else in the hydrocyclone. This provides an everchanging helix-shaped core which was expected through the entire hydrocyclone. The hydrocyclone underflow outlet produced a very unstable flow field in every experiment, due to the transition between the hydrocyclone and the exit hose geometry.

Because the underflow outlet provides an unstable flow field, the CFD model provides a similar pattern at this point, however, this should be considered with caution as the flow is unstable compared to the rest of the hydrocyclone.

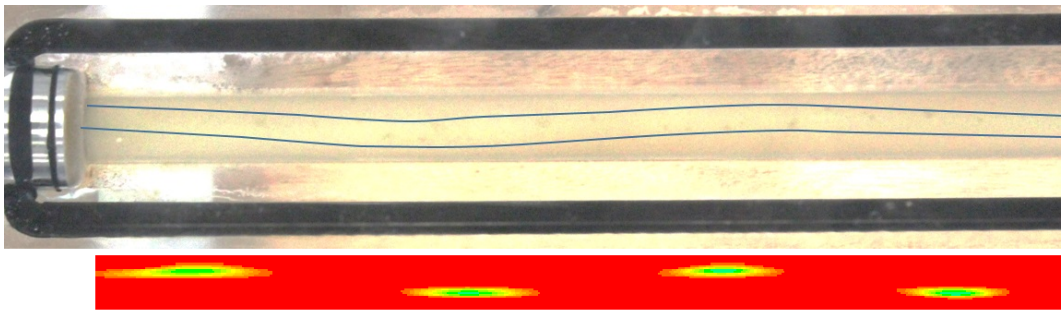

Figure 7.7: Bottom part, oil

7.2 Flow study cases

For the flow study cases, the same convergence criteria is used as in the validation case in section 7.1 page 41. The converged solutions for the cases listed in table 6.4 page 40 is presented in table 7.2. In order to be able to compare the simulation results, the PDR are desired to be as close as possible for each case.

Case	Q_{in}	P_o	P_u	P_i	$\rho_{mixture}$	PDR	$\alpha_{oil,over}$	$\alpha_{water,over}$
#	L/s	kPa	kPa	kPa	kg/m^3	-	%	%
1	0.4	116	146	228	853	1.37	84.4	14.6
2	0.5	126	175	308	844	1.37	89.3	10.7
3	0.6	142	212	403	839	1.37	92.5	7.5
4	0.7	184	282	546	835	1.37	94.7	5.3
5	0.8	205	335	688	832	1.37	96.3	3.7

Table 7.2: Solutions of the flow study cases.

The efficiency of the hydrocyclone is evaluated using the difference between the inlet and underflow outlet oil flow rate as seen in table 7.3, with the efficiency depicted in figure 7.8 page 47.

Case #	$Q_{in,mixture}$ L/s	$Q_{in,oil}$ m^3/h	$Q_{out,oil}$ m^3/h	α_{oil} %	η %
1	0.4	0.072	0.063	3.49	15.2
2	0.5	0.090	0.076	3.41	18.3
3	0.6	0.108	0.080	2.99	35.5
4	0.7	0.126	0.081	2.61	55.2
5	0.8	0.144	0.085	2.37	70.2

Table 7.3: Hydrocyclone efficiency at different flow rates.

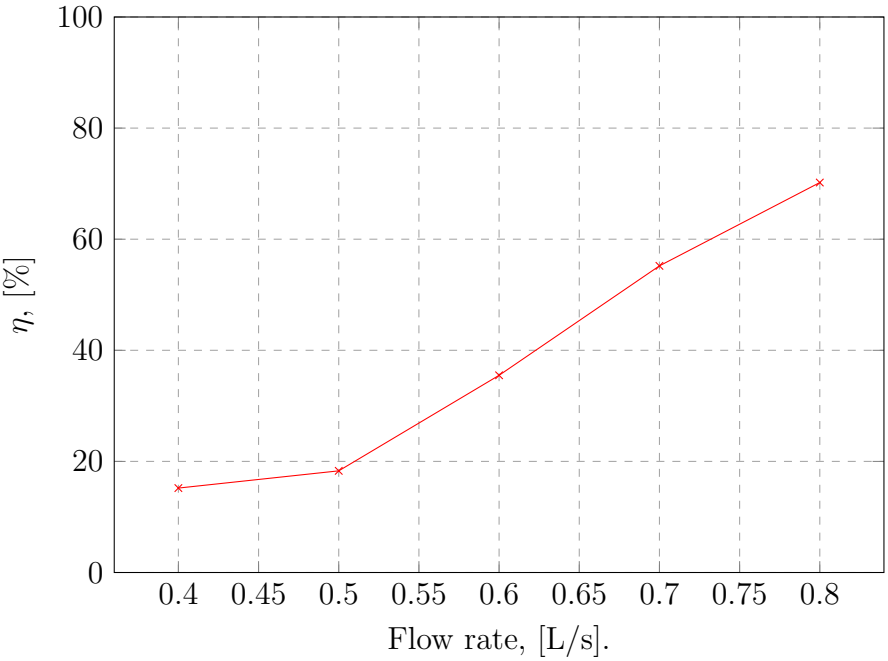

Figure 7.8: Plot of the hydrocyclone efficiency.

Figure 7.8 is consistent with the theoretical flow rate vs efficiency relationship as discussed in section 2.2.2, page 9. Even though the figure from the CFD model is not fully developed and only ranges from 0.4 to 0.8 L/s, the pattern still appear to be true till this point, which points towards a valid CFD model.

7.2.1 Flow study comparison

Several possibilities are available for studying the flow in ANSYS Fluent. Two methods are selected to provide a proper evaluation of the flow field inside the hydrocyclone. These are pointed out in the following itemization.

- Density contour plot
  To provide an overview of the oil and water distribution inside the hydrocyclone.
- Velocity distribution of the flow
  To depict the exact location of the two vortices.

7.2.2 Density contour plots

A set of seven surfaces is created with the purpose of depicting the flow throughout the hydrocyclone. The location of these surfaces are presented on figure 7.9:

Figure 7.9: Location of the seven surfaces inside the hydrocyclone.

For each surface, five density contour plots are depicted to present the flow at the flow rates in case 1 to 5. The part of the figures that shows only water of little interest and is removed to properly compare the details in each of the locations. An example of this is seen in figure 7.10 where the density contour plot is presented for all five cases at the same location:

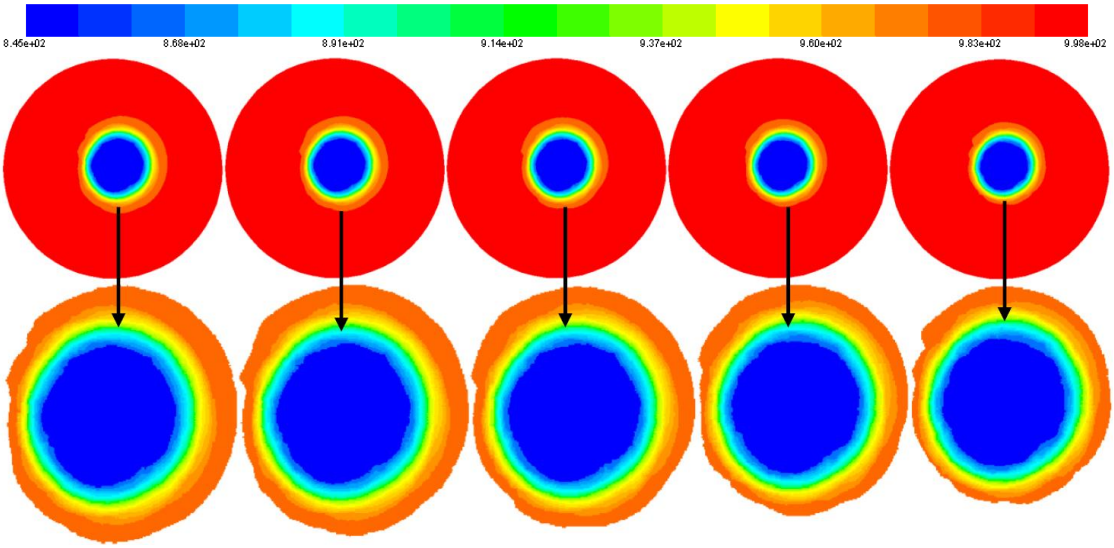

Figure 7.10: The density contour plot from location 1 in case 1 to 5, depicted from left to right.

Figure 7.10 shows no specific differences in the flow field at this specific location by changing the flow rate and this applies throughout the entire hydrocyclone at

all seven locations. For case 1, the plots at these locations are depicted in figure 7.11 page 49.

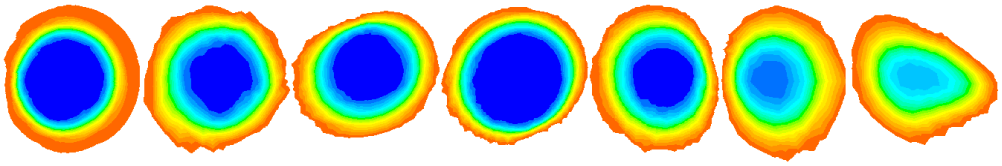

Figure 7.11: The density contour plot at the seven locations through the hydrocyclone with case 1.

The density contour plots from figure 7.11 have been normalized as they all origin from locations with different cross-sectional areas, however, the relative size of the core is the same at all cross-sections.

The further the fluid travels through the hydrocyclone, the more the pressure will drop due to wall friction and the radial velocity will therefore fade. This is basically what is depicted on figure 7.11, where the plot from the last location shows a more mixed fluid and a more skew geometry of the mixture contour plot that includes oil.

7.2.3 Velocity distribution

The velocity distribution inside the hydrocyclone is depicted using the axial velocity. For case 1, the axial velocity distribution of the entire hydrocyclone is depicted in figure 7.12.

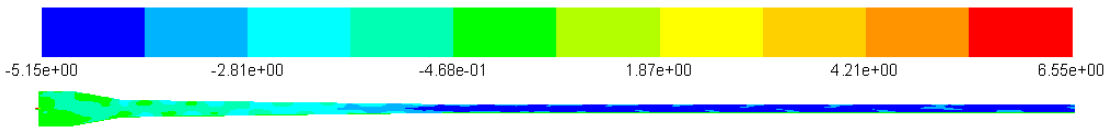

Figure 7.12: The axial velocity in case 1.

The figure points towards the fact that there are no opposite inner vortex and this deviation from the hydrocyclone theory, as explained in section 2.1 page 7, is most likely a result of the hydrocyclone operating outside its ideal operating conditions. This velocity distribution is of the same form in all five cases and therefore this is investigated further.

The colors used to present the magnitudes of the velocity through the hydrocyclone is narrowed down to black for the negative velocities and green for the positive velocities. A positive axial velocity means that the flow is flowing towards the overflow and a negative axial velocity flows towards the underflow. This is depicted in figure 7.13 page 50.

Figure 7.13: The axial velocity in case 1.

It is observed that the velocity is only positive near the inlet and overflow outlet of the hydrocyclone and not through the entire hydrocyclone.

Figure 7.14 shows the difference in axial velocities in the five cases. It must be noted that these are the only positive velocities that exist in the hydrocyclone, and therefore this part of the hydrocyclone is sufficient for comparison. Because this figure is just one plane, it does not present the location where the vortex transporting the mixture to the overflow origins. By transforming the overflow outlet plane, the distance to the origin of the vortices is located as indicated with a red bar on the figure.

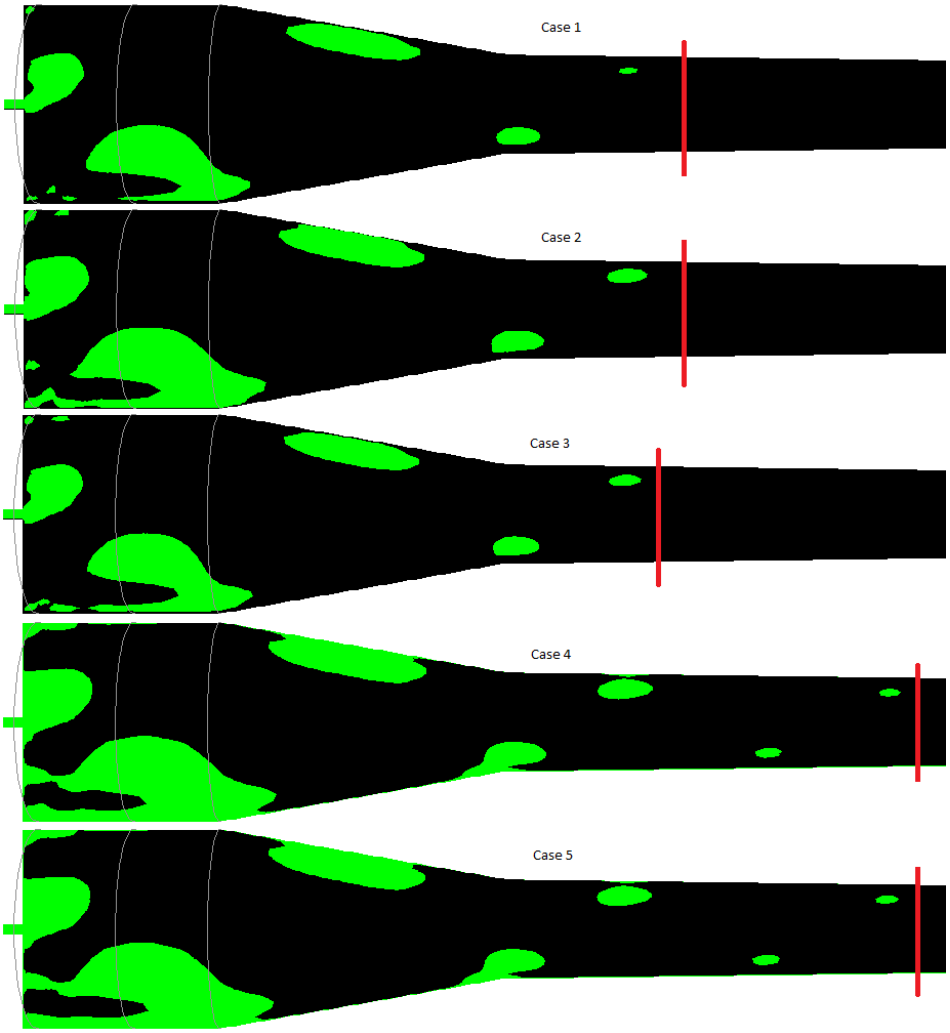

Figure 7.14: The axial velocity in the top section in case 1 to 5.

The pattern of the vortex towards the overflow outlet is the same in every case, where case 1, 2, and 3 shares has a similar length which also goes for case 5 and 6. The pattern of the overflow vortex is the same in all cases and an example from case 5 of this vortex is presented in figures 7.15 and 7.16 page 51.

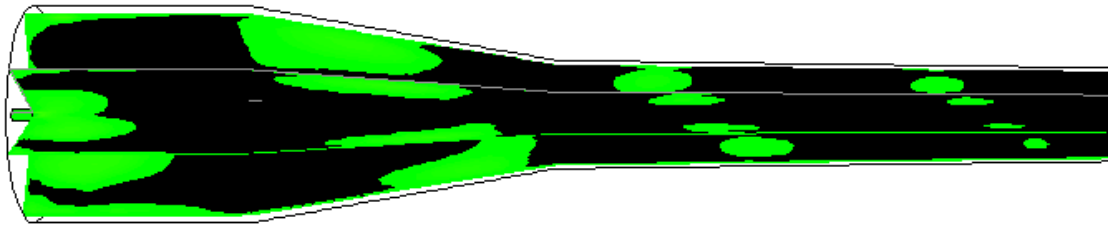

Figure 7.15: The overflow vortex inside the hydrocyclone presented with four planes.

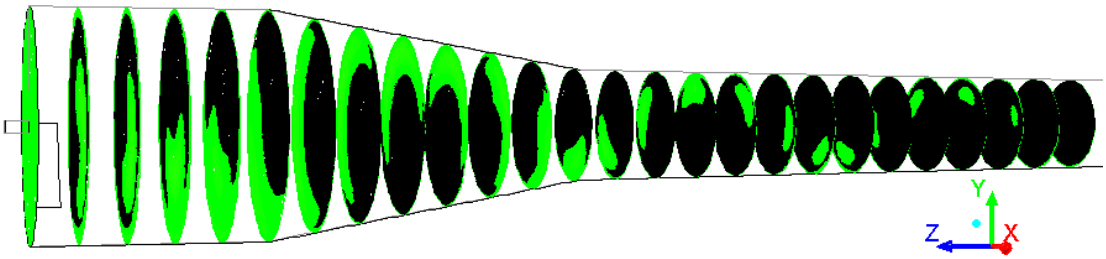

Figure 7.16: The overflow vortex inside the hydrocyclone presented with 26 surfaces.

Figure 7.15 is created by using the same plane form which figure 7.14 is constructed, which is rotated 45°, 90°, and 135°. Basically, this shows that the overflow is created by a vortex which origins in the at a small point relatively close to the inlet in the hydrocyclone and is growing as it approaches the overflow outlet while moving near the wall.

Figure 7.16 is the same case as figure 7.15, but is split up in 26 surfaces with one centimeter between each surface. Here it is clear that the vortex origins roughly 23 centimeters down the hydrocyclone, which is almost 1.5 meters long, and that it spins in a counterclockwise direction. The inlet is seen as at the top of the hydrocyclone and the inlet flow is in the y-direction i.e. clockwise.

Using the density iso-surface plot as presented in figure 7.3 page 43, the locations where oil is caught in the overflow can be determined. Using an iso-surface with a density of 830 kg/m^3, the oil core velocities will be either positive or negative in the axial direction and it can be observed where the oil enters the overflow vortex as presented in figure 7.17 page 52.

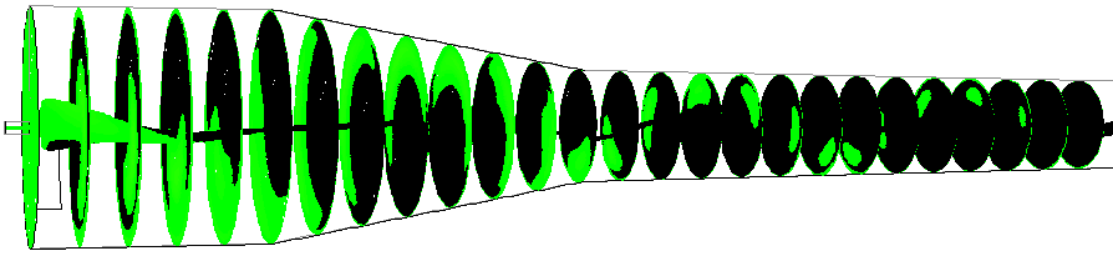

Figure 7.17: The overflow vortex inside the hydrocyclone and the connection to the oil core.

Figure 7.17 shows that the main oil core is only a part of the overflow in the first three centimeters of the hydrocyclone. Because oil is mixed with water through the entire inner axis of the hydrocyclone as presented in section 7.2.2 page 48, an iso-surface with a density close to water is required for a better prediction of where the the oil is collected to the overflow. Therefore, an iso-surface with a mixture density if 985 kg/m^3 is presented in figure 7.18, as this is the closest achievable value to depict with ANSYS Fluent without getting a fatal error.

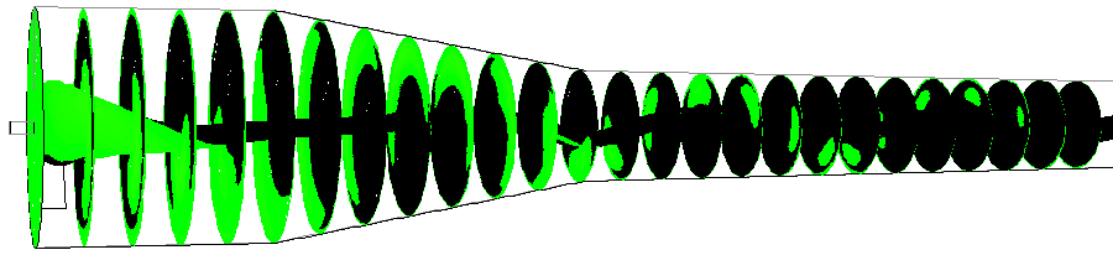

Figure 7.18: The overflow vortex inside the hydrocyclone and the connection oil-water mixture core.

In this hydrocyclone with an inlet flow rate of 0.8 L/s, the oil is collected in the overflow vortex in around 12 centimeters down the hydrocyclone. Adjusting the flow rate into the hydrocyclone will reduce the size of the overflow vortex which can be seen in figure 7.14 page 50, and this also explains the reason for an increased efficiency when increasing the flow rate. Figure 7.16, 7.17, and 7.18 is presented for all five cases in appendix F.

8 Discussion

8.1 Experiments

The experiments conducted for this master thesis did not turn out as initially planned. The idea was to test a range of flow rates in the hydrocyclone setup and compare each experiment with a CFD model. However, the laboratory setup did not allow the possibility of including oil to the flow in a proper manner to begin with, and the only method for measuring the oil fraction in the mixture was a coriolis flow meter located at the overflow outlet. After a period of time, the oil pump was connected to the system with an oil tank to allow the possibility of mixing water and oil. The maximum possible flow rate the system could provide was roughly 0.7 L/s due to the restrictions in the system which includes a maximum pressure at 5.5 bar after the water pump.

Because the system setup was barely suitable for the desired experiments and a maximum of only 200 liters of oil were available, only one experiment could be conducted, which would be the CFD model validation case. While conducting this experiment, most of the tests did not contain useful data as the water pump shut down for short periods of time several times in 10 of the 12 tests. Luckily the remaining two tests were test 9 and 10, which opened up for the possibility to collect data from test 10, as test 9 was used to fill the system with the right oil-water mixture.

8.1.1 Validation case

The results, using the outlet pressures from the experiment in the CFD model, yielded a pressure difference of 49 kPa, but only an overflow density difference of 1.4 kg/m^3 and ultimately a difference in PDR of only 0.01 as shown in table 8.1.

	ρ	P_i	PDR
	kg/m^3	kPa	-
Experiment	926.8	414	1.19
CFD model	928.2	463	1.18

Table 8.1: Validation case experimental and CFD data.

The pressure difference between the experiment and the CFD model can be the result of the y$^+$ values which are unfit for the available wall functions which can contribute to a misinterpretation of the wall friction. If this is the case, this

problem may be solved by re-meshing the hydrocyclone to achieve a more suitable y^+ value.

Despite the disagreement regarding the inlet pressure, the CFD model are still considered suitable for modeling the hydrocyclone as the PDR barely varies and are one of the most important factors for achieving proper results which is also seen in the density which is close to reality.

8.1.2 Visual documentation

The photographs and video from the experiment will not be in shape to be used for comparison with the CFD model. It is not possible to see the density distribution in a photograph and the size of the inner vortex may not be of the same size as the oil core that is visible. A CFD model will always show the results and flow under optimal operating conditions as oppose to an laboratory setup which will not be able to maintain e.g. a constant water flow rate.

What might appear to be a stationary oil core will include small fluctuations and the inner vortex can be located both inside and outside the oil core and may therefore not be visible due to a blurry flow.

8.2 Droplet size

The droplet size used in the CFD model is determined experimentally and is therefore a mean value of the particle sizes in the oil mixture. A hydrocyclone is able to separate droplet down to a size of approximately 40μm, depending on the hydrocyclone model, while the average droplet size in this oil was found to be 400μm. In an industrial setup, the mixture will enter the hydrocyclone after being separated in a large separation tank and therefore only lead smaller particles to the hydrocyclone.

Because any de-oiling hydrocyclone will be able to separate oil droplets with a size of 400μm the CFD simulations will not be a fully realistic case. In order to achieve this, the droplet size range must be known and used as input along with the void fraction.

The assumption of all droplets being the same size may lead to a higher simulated efficiency than possible in the real hydrocyclone.

8.3 Flow field study

As revealed in section 7.2.3 page 49 the CFD simulation revealed a different hydrocyclone flow field than described in the theory.

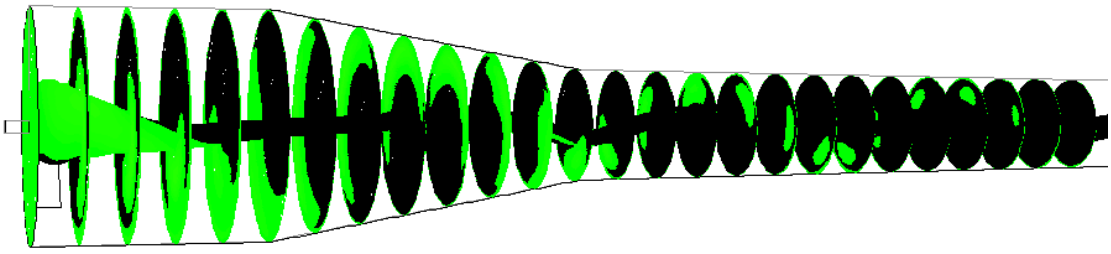

Figure 8.1: The overflow vortex inside the hydrocyclone and the connection oil-water mixture core.

It is revealed that there is an oil core in the center of the hydrocyclone as expected, but the inner and outer vortices are not located as such. This shows a hydrocyclone flow field when it is performing poorly due to flow rates being below the minimum required to maximize the efficiency as depicted in figure 8.3.

Assuming the CFD simulation predicts the flow field realistically, the assumption of the y^+ values being of little importance may no longer be valid. The intention was to evaluate the flow with an inner and outer vortex through the entire hydrocyclone where the interaction between these were of interest and not the water-wall interaction. At this point the overflow vortex is developed relatively close to the inlet near the wall and is therefore affected by both the wall- and phase friction.

The effect of PDR has not been studied in this project and the value of roughly 1.37 used in the CFD simulations is relatively low compared to the typical value between 1.5 and 3. An increased PDR may alter the flow field and will change the location of where the overflow vortex origins, however the impact of an increased PDR is not investigated, so this is up for future work on this subject.

Even with a different flow field than expected from going through hydrocyclone theory, the flow rate-efficiency relationship still follows the expected pattern.

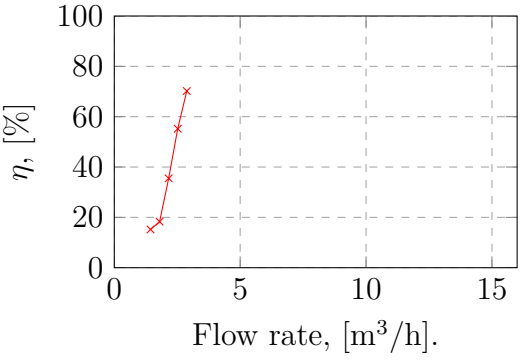

Figure 8.2: Plot of the hydrocyclone efficiency.

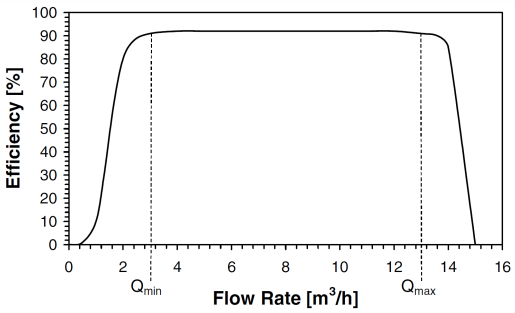

Figure 8.3: Typical hydrocyclone efficiency versus flow rate relationship[3].

At this point there has not been sufficient time to make enough simulations to depict a larger flow rate span and it is therefore not possible to determine the flow rate which provides the best possible separation for this specific hydrocyclone.

9 Conclusion

The purpose of this project has been to study the flow field inside a de-oiling hydrocyclone while operating it under different flow rates leading to non-optimal conditions. Flow rates from 0.4 to 0.8 L/s have been modeled in ANSYS Fluent and the model has been verified with an experiment in the laboratory at Aalborg University in Esbjerg.

In the validation experiment the overflow density and inlet pressure was used as validation parameter. The mixture density in the overflow were measured to be 926.8 kg/m^3 and the CFD model were 1.4 kg/m^3 higher. The inlet pressure were measured to me 414 kPa as oppose to 463 kPa in the CFD model, which initially seems like a notable difference, however the PDR is only 0.01 off. Therefore the validation experiment is concluded successful and the CFD model were used for further study of the flow field.

It was not possible to properly compare the experimental flow field to the CFD model in detail due to the visibility in the hydrocyclone when the oil and water were mixed. Therefore the flow field has not been considered an important validation parameter.

The flow field study made it possible to draw several conclusions. A flow rate-efficiency relationship has been developed which proves that an increasing flow rate provides a higher efficiency. The optimal flow rate for this hydrocyclone were unfortunately not determined as time did not allow for it, but it follows the theoretical pattern for the flow rate-efficiency relationship when operating below Q_{min}. A PDR of 1.37 has been used for every simulation to determine the effect of a changing flow rate. An initial flow rate of 0.4 L/s in the hydrocyclone had an efficiency of 15.2%, while increasing the flow rate to 0.8 L/s also increased the efficiency to 70.2%.

It was expected to see an inner vortex, with the length of the full hydrocyclone, which would carry the oil through the hydrocyclone and leave the hydrocyclone at the overflow outlet. However, because the hydrocyclone is not operating under ideal conditions, the flow field is not the same. It was observed that the overflow vortex has its origin relatively close to the inlet and that it flowing near the wall while moving towards the overflow outlet as seen in figure 9.1 page 58.

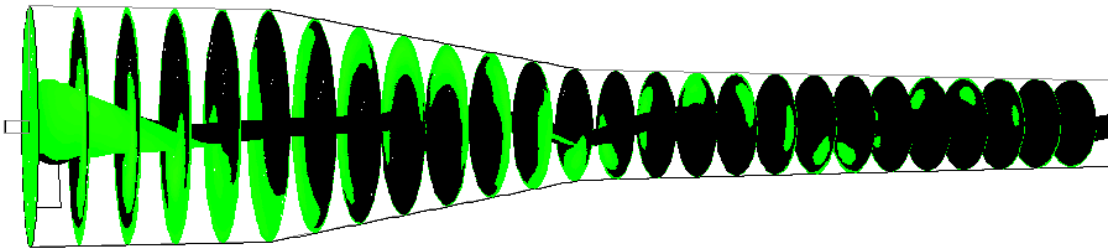

Figure 9.1: The overflow vortex inside the hydrocyclone and the connection oil-water mixture core.

Oil is still being forced to the center of the hydrocyclone as expected, but is moving with a negative axial velocity and is only being transfered to the overflow where the overflow vortex and the oil core connects. Therefore it can be concluded that an increasing flow rate will increase the width and length of the overflow vortex, resulting in a larger connection area with the oil core and therefore a higher efficiency. This concludes that the flow rate, vortex width and length, and efficiency are connected and follows the previously discussed relationship as depicted in figure 9.2.

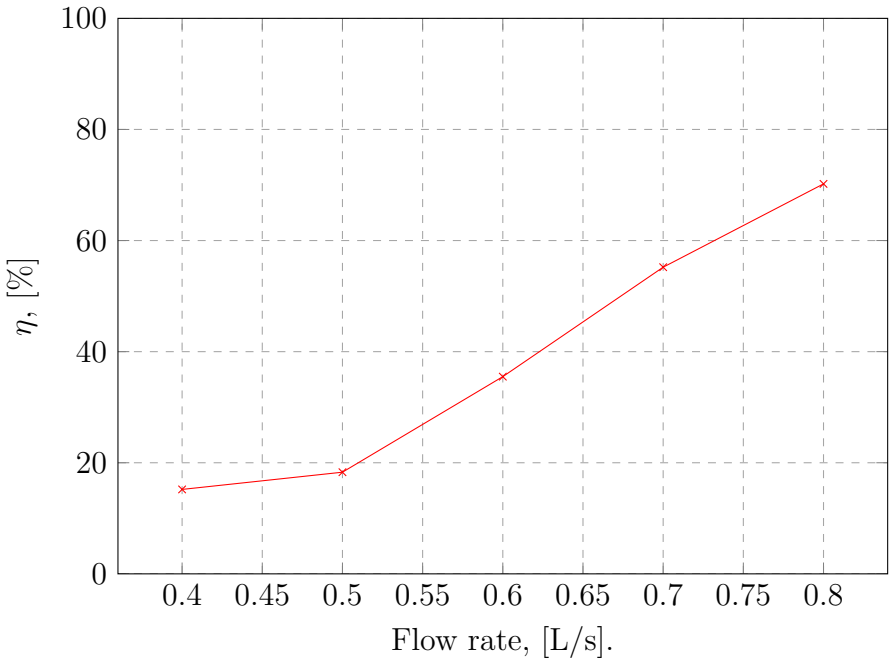

Figure 9.2: Plot of the hydrocyclone efficiency.

Suggestions for future work

A suggestion for future work is to produce a complete flow rate-efficiency graph for hydrocyclones when not operating under optimal settings. A realistic droplet size range will be desired to achieve the best result instead of using a set droplet size averaged from oil that have not been through a separation tank.

A study on the flow field while operating under different Pressure Drop Ratios will also be a possibility for future work.

Bibliography

[1] Steve Tarletom. *Progress in Filtration and Separation*. Academic Press, 2015.

[2] A. B. Sinker, M. Humphris, and N. Wayth. Enhanced deoiling hydrocyclone performance without resorting to chemicals. 1999.

[3] Trygve Husveg, Odile Rambeau, Tormod Drengstig, and Torleiv Bilstad. Performance of a deoiling hydrocyclone during variable flow rates. *Minerals Engineering*, 20:368–379, 2007.

[4] S. Noroozi and S.H. Hashemabadi. Cfd analysis of inlet chamber body profile effects on de-oiling hydrocyclone efficiency. *Chemical Engineering Research and Design*, 89:968–977, 2011.

[5] Y. Rama Murthy and K. Udaya Bhaskar. Parametric CFD studies on hydrocyclone. *Powder Technology*, 230:36–47, 2012.

[6] K. Udaya Bhaskar, Y. Rama Murthy, M. Ravi Raju, Sumit Tiwari, J.K. Srivastava, and N. Ramakrishnan. CFD simulation and experimental validation studies on hydrocyclone. *Minerals Engineering*, 20:60–71, 2007.

[7] T.J. Olson and R. Van Ommen. Optimizing hydrocyclone design using advanced CFD model. *Minerals Engineering*, 17:713–720, 2004.

[8] Safa Razuteh and Soltani Goharrizi Ataallah. CFD simulation of an industrian hydrocyclone with Eulerian-Eulerian approach: A case study. *International Journal of Mining Science and Technology*, 24:643–648, 2014.

[9] H K Versteeg and W Malalasekera. *An Indroduction to COMPUTATIONAL FLUID DYNAMICS The Finite Volume Method, second edition*. Pearson Education Limited, 2007.

[10] Mikko Manninen and Veikko Taivassalo. On the mixture model for multiphase flow. *VTT PUBLICATIONS*, 288, 1996.

[11] ANSYS Inc. ANSYS Fluent Theory Guide, 2013.

[12] Abdulnaser Sayna. *Computational Fluid Dynamics, first edition*. bookboon, 2009.

[13] VirginiaTech. Using Flow Boundary Conditions. http://www.arc.vt.edu/ansys_help/flu_ug/x1-4300008.63.2.html.

[14] Munson, Okiishi, Huebsch, and Rothmayer. *Fluid Mechanics, seventh edition*. Wiley, 2013.

[15] Michael Skov Bjerre, Jacob Gram Iskov Eriksen, Frank Bjerre Sørensen, and Olli Aleksanteri Haavikko. CFD Simulation of Coriolis Flow Meter. 2013.

[16] ANSYS Inc. ANSYS Fluent User's Guide, 2013.

[17] Sandia National Laboratories. CUBIT. https://cubit.sandia.gov/.

[18] Michael Casey and Torsten Wintersgerste. ERCOFTAC Special Interest Group on "Quality and Trust in Industrian CFD" Best Practice Guidelines.

[19] GAMBIT. GAMBIT 2.4 User's Guide, May 2007.

A P&ID of the full laboratory setup

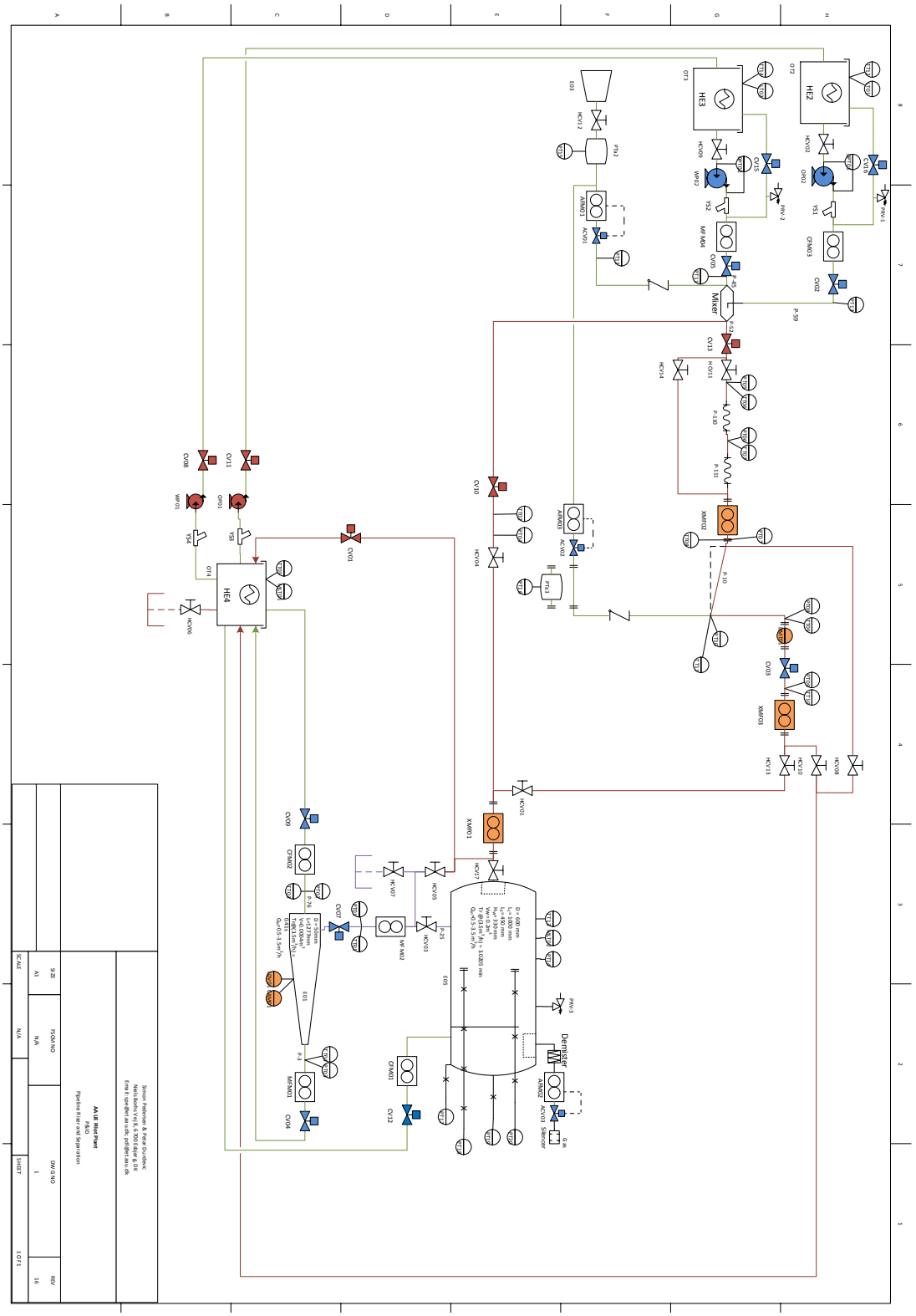

B Oil density experiment

B.1 Purpose of the oil density experiment

The purpose of the experiment is to determine the density of the oil used for the experiments regarding the hydrocyclone.

B.2 Materials and equipment

The following material is used:

- SAE 30 mineral oil from *ardeca Lubricants*

The following equipment is used:

- Weight scale
- 1 L Measuring beaker

B.3 Methods

1) The weight of the beaker is determined.
2) 500 mL oil is collected in the measuring beaker.
3) The weight of the beaker with oil is determined and the differential weight is the mass of 0.5 L oil.

The experiment setup is shown in figure B.1 page 65.

Figure B.1: 0.5 L oil on a weight scale for oil density determination.

B.4 Measuring error

The indication on the measuring beaker is relatively rough and therefore an exact result cannot be found. The error is assumed to be ±5 mL, i.e. 495-505 mL.

B.5 Results and discussion of the experimental data

- $m_{beaker} = 270.70g = 0.27070kg$
- $m_{beaker+oil} = 683.88g = 0.68389kg$
- $m_{oil} = 413.19g = 0.41319kg$

The mass of the oil is 0.41319 kg for 500 mL i.e. 0.82628 kg/L ±0.008 kg/L.

The density measuring error should be taken into consideration, however because only one value for the density can be used for the simulation, the mean value is taken. The oil density for the simulations is therefore determined to be:

$$\rho_{oil} = 826\ kg/m^3 \tag{B.1}$$

C Droplet study

Input data is set up to recreate the oil-water experiment.

Turbulence model	$k-\varepsilon$, RNG, Standard wall function
Solution algorithm	PISO
Discretization scheme	QUICK
Solver	Incompressible, transient
Inlet BC	Velocity inlet, 14.839 m/s
Overflow outlet BC	Pressure outlet, 187870 Pa
Underflow outlet BC	Pressure outlet, 229600 Pa
Oil fraction	2.3%

Table C.1: Selected solution parameters for the droplet size study.

The mixture density in the overflow was determined in section 5.5, 35 to be $926.8 kg/m^3$. Meanwhile, the oil fraction was calculated to be 2.3%.

The particle size was adapted in ANSYS fluent until the simulation produced an overflow mixture density as close to the experimental results as possible. Fortunately, a good enough value for the droplet size were achieved after two attempts after a 10 second transient simulation. The cases that were tested was with a droplet size of initially 40μm and finally 400μm. The data acquired for these simulations are presented in table C.2.

Droplet size μ**m**	**Density** **kg/m**^{3}
40	973.8
400	928.2

Table C.2: The results of the droplet size study.

The droplet size used for further simulations will therefore be 400μm.

The simulation residual plot is presented in figure C.1 page 67.

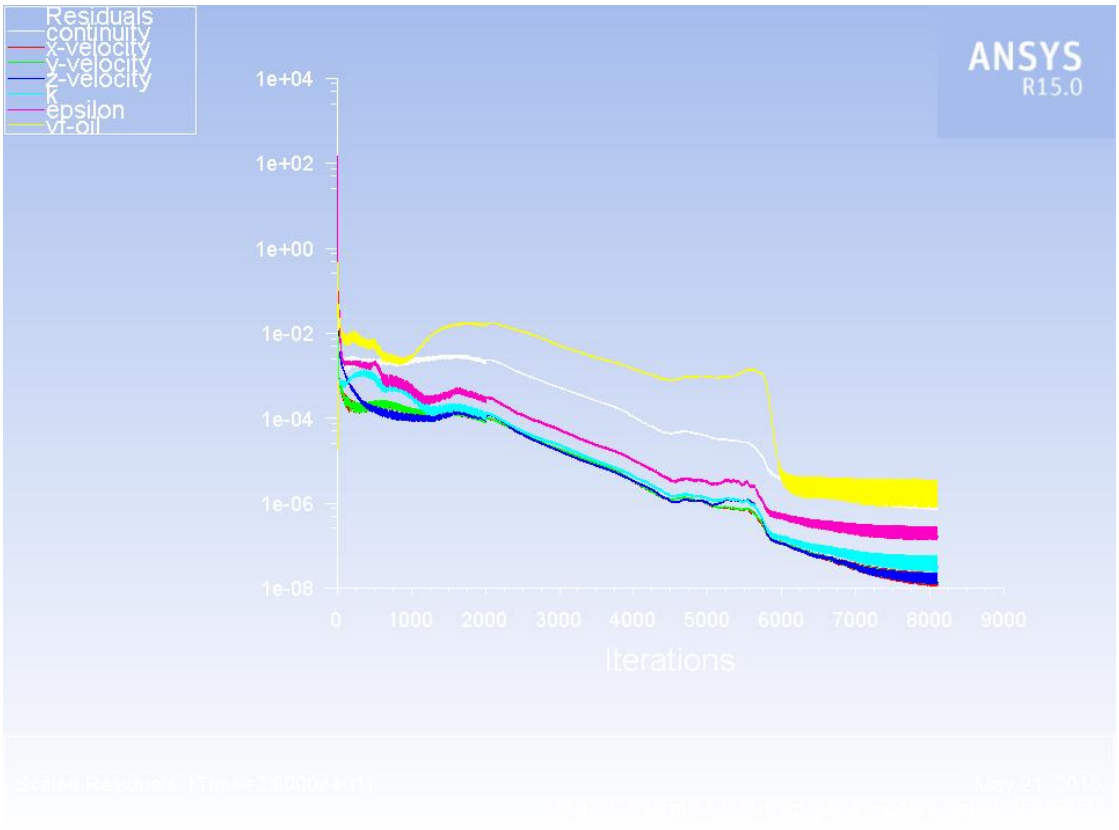

Figure C.1: The residual plot of the droplet study simulation.

D The SIMPLE algorithm

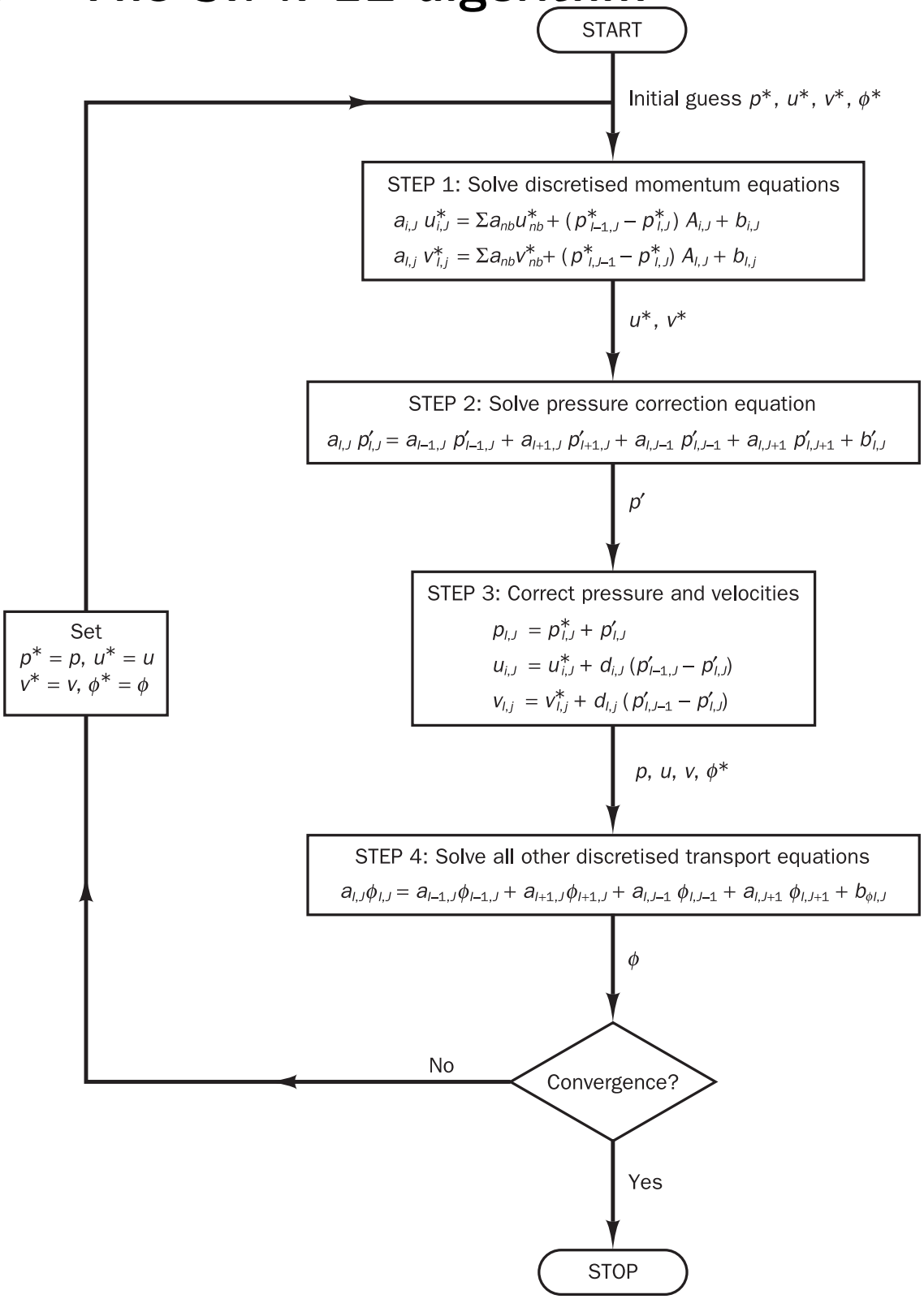

E The PISO algorithm

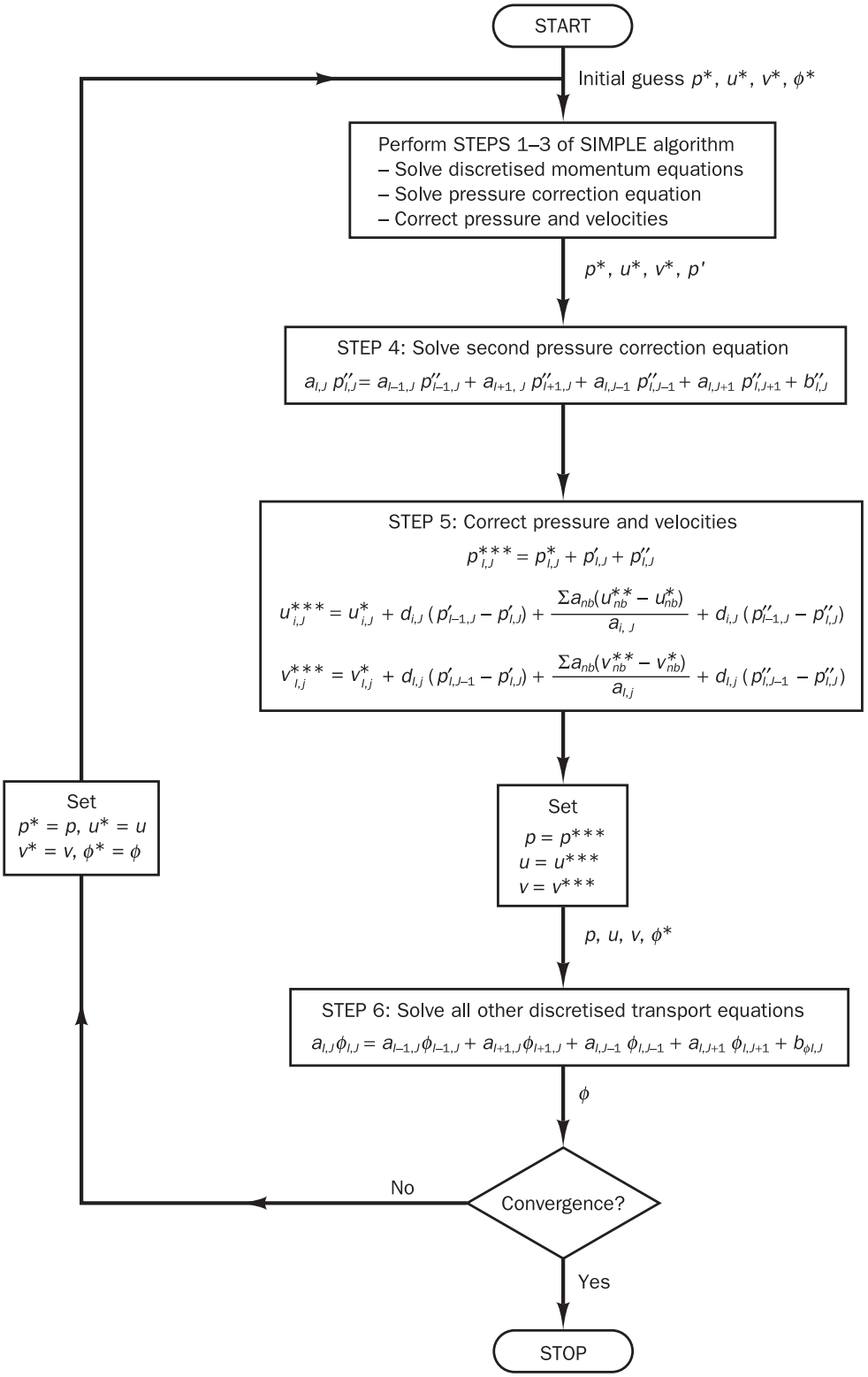

F Overflow vortex and oil connections

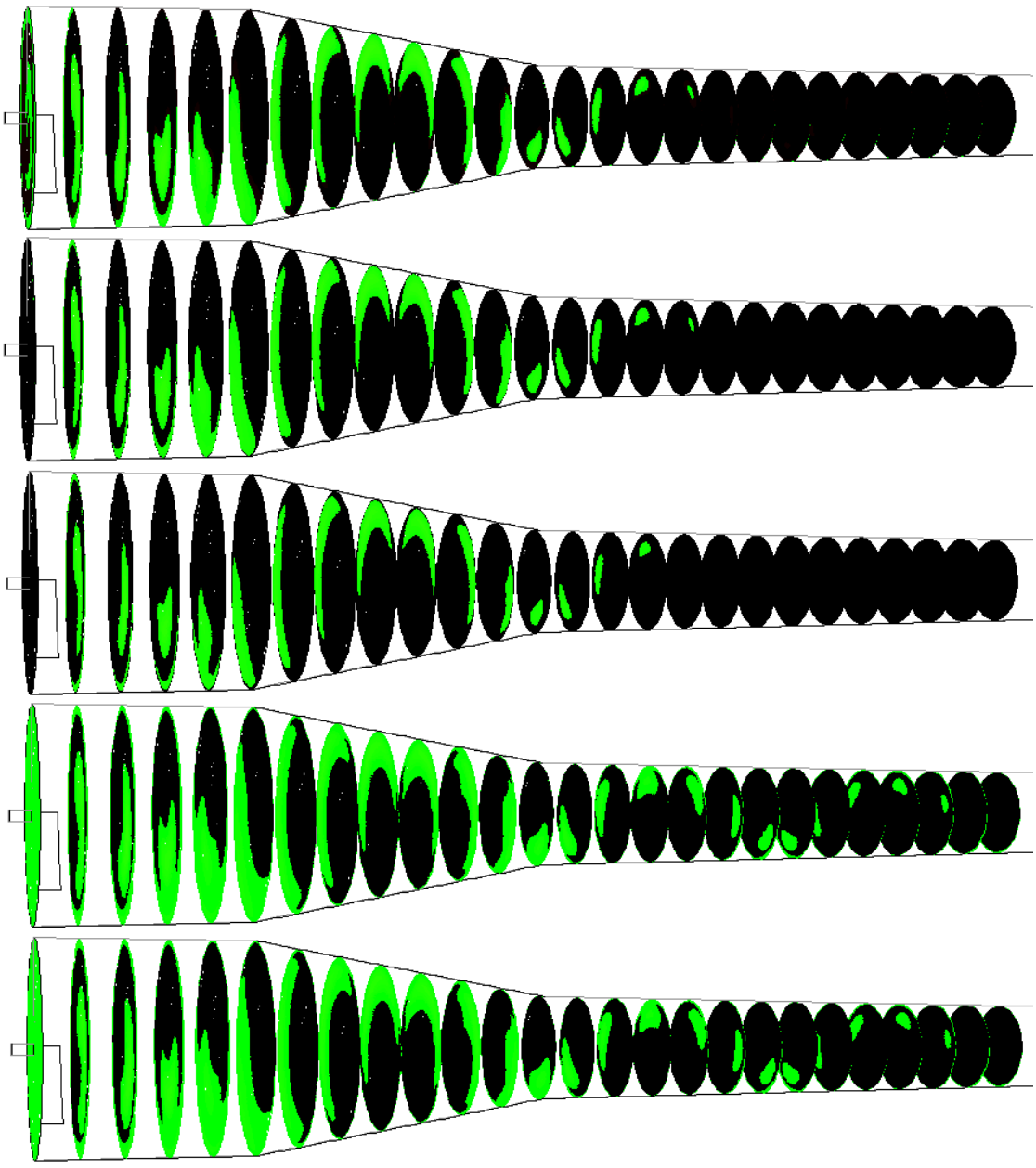

Figure F.1: The overflow vortex in case 1 to 5.

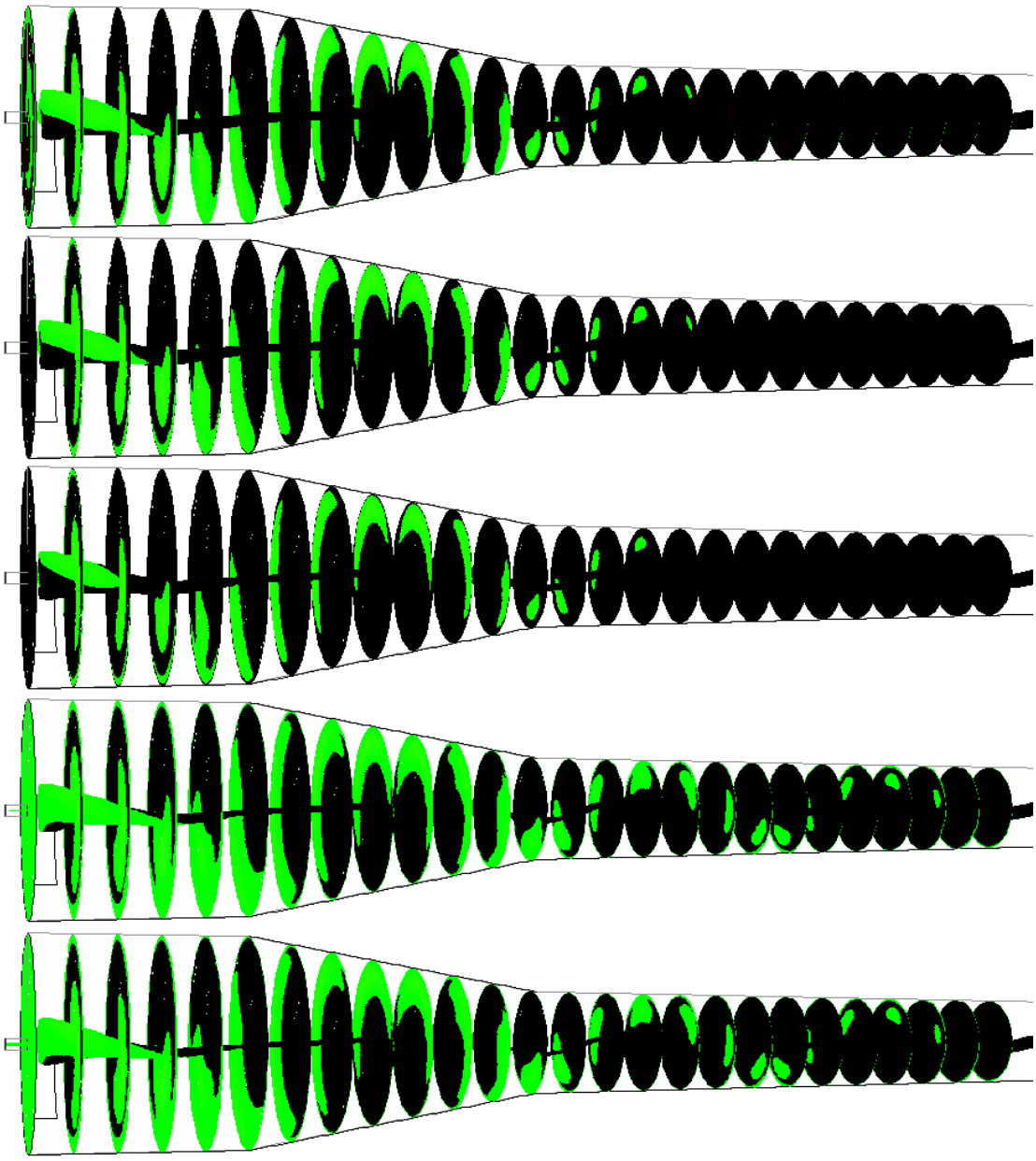

Figure F.2: Oil connection to the overflow vortex with a iso-surface with a density of 830 kg/m^3.

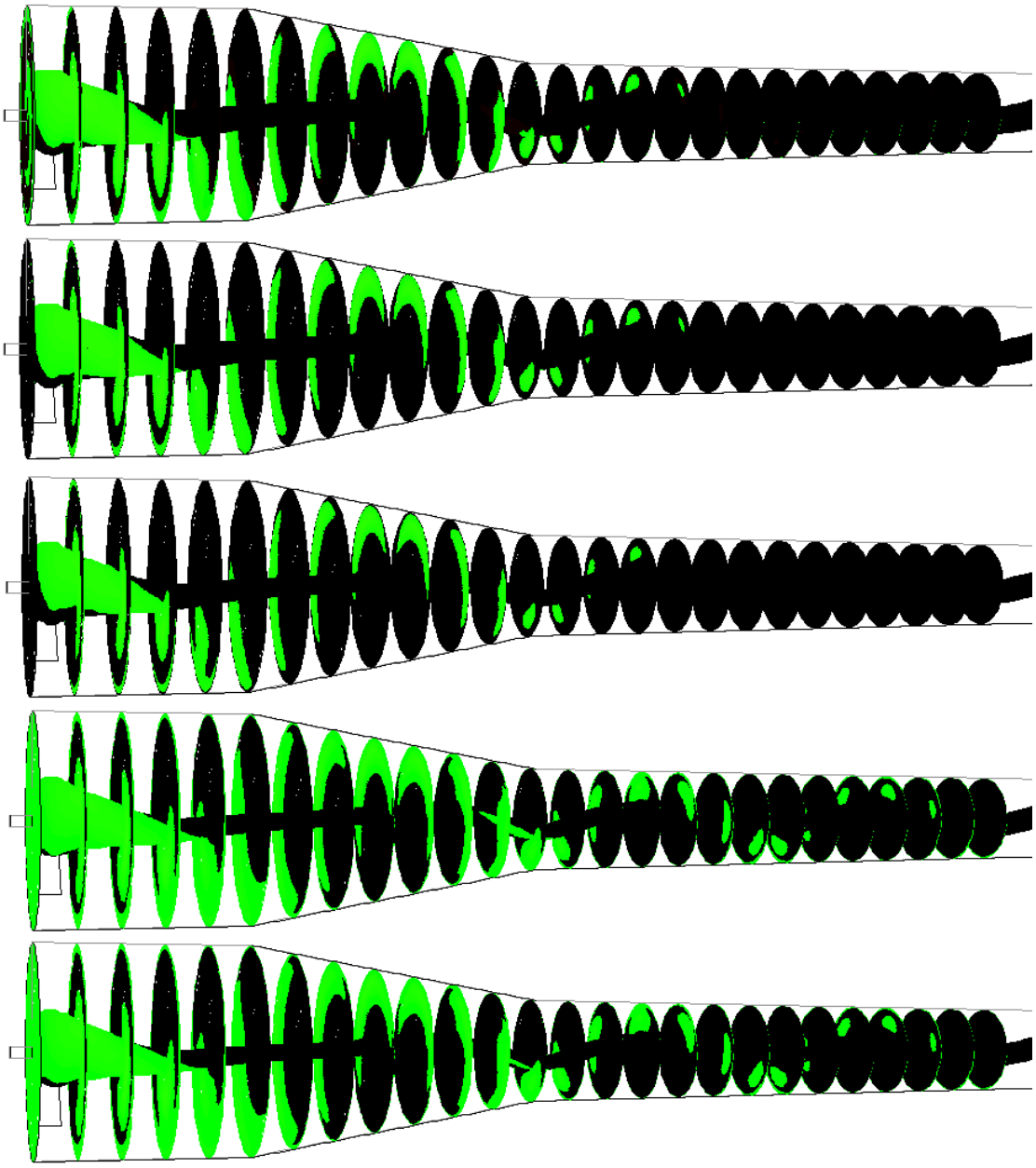

Figure F.3: Oil connection to the overflow vortex with a iso-surface with a density of 985 kg/m^3.